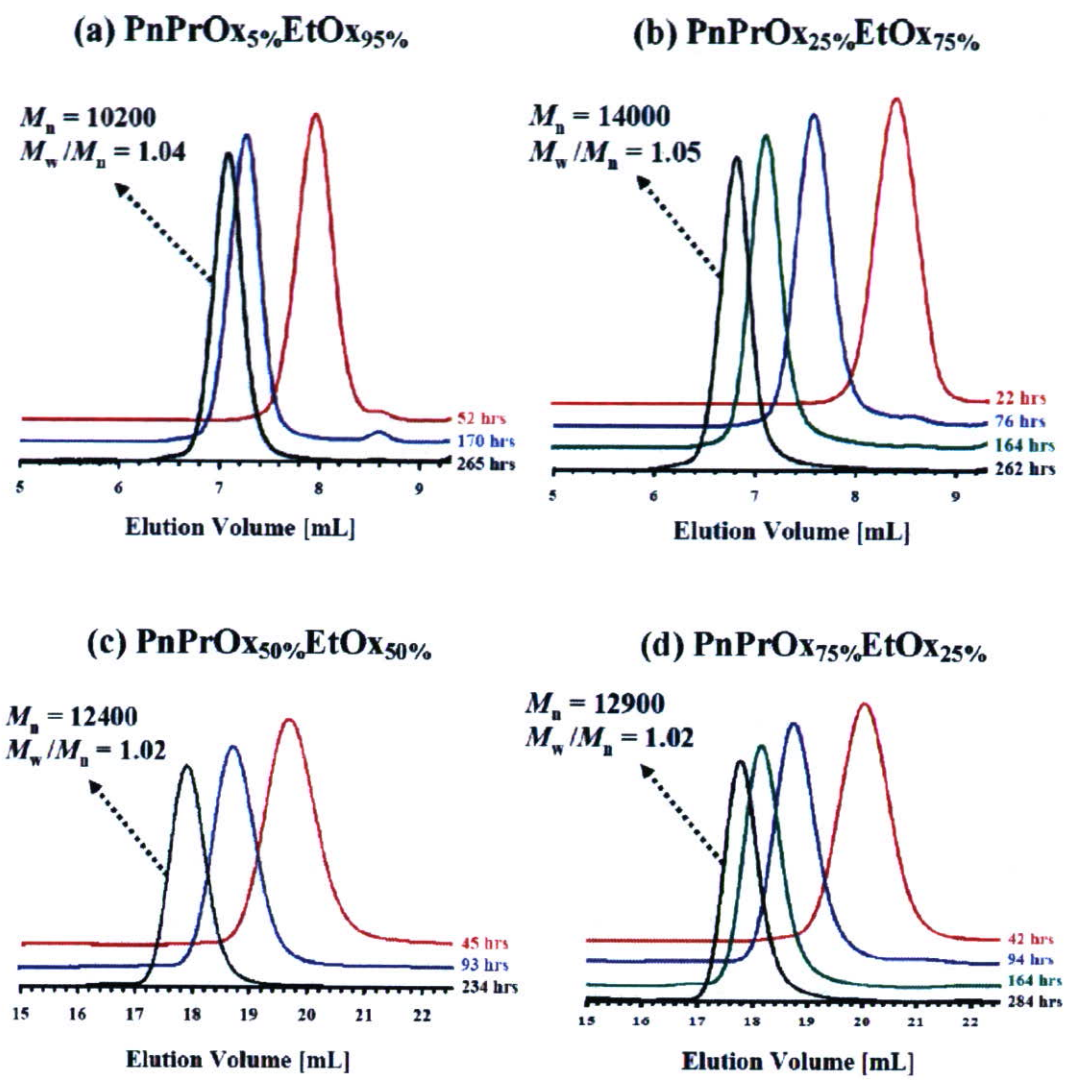

Figure 7. GPC traces of four random copolymers ((a) P*n*PrOx$_{5\%}$EtOx$_{95\%}$, (b) P*n*PrOx$_{25\%}$EtOx$_{75\%}$, (c) P*n*PrOx$_{50\%}$EtOx$_{50\%}$, and (d) P*n*PrOx$_{75\%}$-EtOx$_{25\%}$) having different molecular weights (column, SuperAW4000 and SuperAW3000 (a, b) and G4000H$_{HR}$ and G3000H$_{HR}$ (c, d); P*i*PrOx standard; eluent, DMF (containing 10 mM LiCl and 30 mM TEA); temperature, 40 °C; RI detection).

random copolymers comprising *n*PrOx and EtOx in order to explore the phase transition behavior of the P(*n*PrOx-*ran*-EtOx) copolymers without the *i*PrOx component (Scheme 1). The respective mixtures of 2-*n*-propyl-2-oxazoline (*n*PrOx$_{5\%}$, 1.11 mmol; *n*PrOx$_{25\%}$, 5.53 mmol; *n*PrOx$_{50\%}$, 11.1 mmol; *n*PrOx$_{75\%}$, 16.6 mmol) and 2-ethyl-2-oxazoline (EtOx$_{95\%}$, 21.0 mmol; EtOx$_{75\%}$, 16.6 mmol; EtOx$_{50\%}$, 11.1 mmol; EtOx$_{25\%}$, 5.53 mmol) were added to a solution of MeOTs (0.250 mmol) in acetonitrile and polymerized at 42 °C, as in the case of the two homopolymers (P*n*PrOx and PEtOx). The synthesis results of four copolymers (P*n*PrOx$_{5\%}$EtOx$_{95\%}$, P*n*PrOx$_{25\%}$EtOx$_{75\%}$, P*n*PrOx$_{50\%}$-EtOx$_{50\%}$, and P*n*PrOx$_{75\%}$EtOx$_{25\%}$) with the same initial monomer/initiator ratio (DP$_{calcd}$ = 88.4) are summarized in Table 2. The polymerization behaviors of the copolymers with the initial *n*PrOx and EtOx molar ratios of 5%:95%, 25%:75%, 50%:50%, and 75%:25% were characterized by the time-dependent change in the DP and PDI via the MALDI−TOF mass and GPC traces, as seen in Figures 6 and 7. Regardless of the comonomer ratio in the feed, the experimental degree of polymerization (DP from MALDI−TOF mass spectrometry) of the respective copolymers was close to the predicted value from the initial monomer/initiator ratio (DP$_{calcd}$ = 88.4) and their molecular weight distributions were quite narrow (Figure 6). The GPC traces of the four copolymers with different monomer ratios in the feed (P*n*PrOx$_{5\%}$EtOx$_{95\%}$, P*n*PrOx$_{25\%}$EtOx$_{75\%}$, P*n*PrOx$_{50\%}$EtOx$_{50\%}$, and P*n*PrOx$_{75\%}$EtOx$_{25\%}$), which were sampled at different polymerization times, also showed an increase in the molar mass with time and symmetrical monomodal peaks, as shown in Figure 7a−d. In addition, the compositions of the final copolymer products determined by ^{1}H NMR spectrometry were almost in good agreement with the calculated values from the feed ratio of both monomers, indicating their quantitative conversion into the respective copolymers (Figure 8 and Table 2).

In this living polymerization system, the copolymers were expected to form a random composition, providing similar reactivity ratios of the two monomers, *n*PrOx and EtOx. Indeed, from the composition analysis by ^{1}H NMR spectrometry of the respective copolymer samplings (monomer conversions: ca. 20−40%) plotted in Figure 6, the reactivity ratios of the respective monomers were calculated to be $r_{n\mathrm{PrOx}} = 1.28$ and $r_{\mathrm{EtOx}} = 1.04$ using the nonlinear Tidwell−Mortimer (TM) method.[16] This similarity in the reactivity ratios of two monomers indicates that both *n*PrOx and EtOx should be introduced into the copolymer backbone at almost an equal rate. Because of the simultaneous initiation and uniform propagation

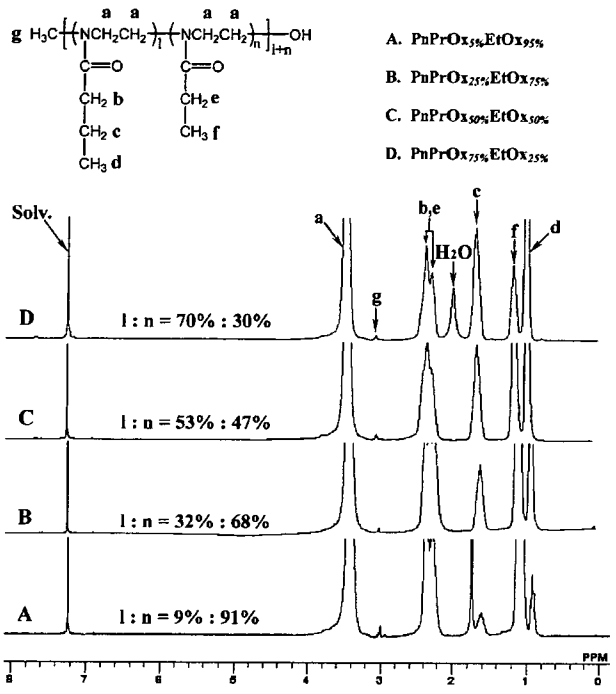

Figure 8. ^{1}H NMR spectra for the final products of the four random copolymers (P*n*PrOx$_{5\%}$EtOx$_{95\%}$, P*n*PrOx$_{25\%}$EtOx$_{75\%}$, P*n*PrOx$_{50\%}$EtOx$_{50\%}$, and P*n*PrOx$_{75\%}$EtOx$_{25\%}$) in $CDCl_3$ at 25 °C.

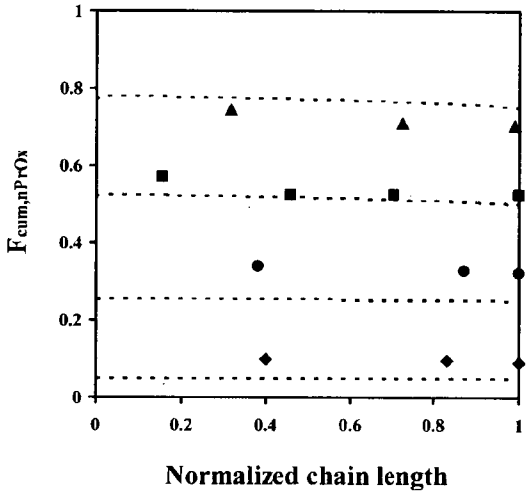

Figure 9. Cumulative ($F_{cum,nPrOx}$) composition plots for random copolymers. The theoretical prediction curves (dotted) were calculated using the simulation program PROCOP[17] (P*n*PrOx$_{5\%}$EtOx$_{95\%}$ (◆), P*n*PrOx$_{25\%}$EtOx$_{75\%}$ (●), P*n*PrOx$_{50\%}$EtOx$_{50\%}$ (■), and P*n*PrOx$_{75\%}$EtOx$_{25\%}$ (▲)).

kinetics in this living system as known from the extremely low polydispersity indices, each polymer chain should exhibit a similar composition ratio of *n*PrOx and EtOx along the backbone from the α-terminal to active ω-chain end. The cumulative composition plots ($F_{cum,nPrOx}$) vs the normalized chain length were obtained for the four copolymerizations with different initial molar ratios of *n*PrOx and EtOx in the feed (Figure 9). According to the experimental plots, the shape of the obtained random copolymers almost followed the theoretical curves using $r_{nPrOx} = 1.28$ and $r_{iPrOx} = 1.04$.[18]

In addition, a series of MALDI−TOF mass spectra for P*n*PrOx$_{50\%}$EtOx$_{50\%}$, which were sampled at different polymerization times, were obtained as shown in Figure 10, showing a good coincidence with the result of the GPC trace. The MALDI−TOF mass spectrometry thus provided quantitative information about the sequence and composition present in the copolymer when compared to the theoretical mass values and relative intensities for a specific copolymer with the experimental mass spectrum.[19] The series of all the copolymer samplings with the chain lengths below ca. $M_n = 10\,000$ could provide comparatively clearer mass spectra, and the enlarged mass spectrum of P*n*PrOx$_{50\%}$EtOx$_{50\%}$ sampled after 17 h was selected for a detailed analysis of copolymer composition and sequence distribution (Figure 10). All the peaks shown in the mass spectrum of Figure 10 were assigned to copolymers comprised of the *n*PrOx and EtOx monomer units with both methyl groups at the α-terminals and hydroxyl groups at the ω-terminals. The calculated mass of each copolymer was expressed by the following equation:

$$\begin{aligned}\text{Mass}_{calcd} &= [n\text{PrOx}]_{l-\text{mers}} + [\text{EtOx}]_{n-\text{mers}} \\ &= \Delta[n\text{PrOx}]l + \Delta[\text{EtOx}]n + [\alpha\text{-methyl and} \\ &\quad \omega\text{-hydroxyl groups}] + [\text{Na}^+]\end{aligned}$$

($\text{Mass}_{calcd}(m/z)$; the calculated mass of a copolymer with the degree of polymerization nearest to the measured value, Δ[*n*PrOx] (or Δ[EtOx]); the mass of the monomer unit, [Na^+]; the mass of sodium ion.) The detailed peak assignments are summarized in Table 3 in which Mass_{expt} is the experimental mass value of the most and second intense signals among the respective homologue series in the mass region of 1200−1900. For instance, the strongest signal ($\text{Mass}_{expt} = 1554.36$) and second most intense signal ($\text{Mass}_{expt} = 1540.12$) in the mass region of 1500−1600 almost agreed with the calculated mass values of the two corresponding copolymers as shown below.

$$[n\text{PrOx}]_{8-\text{mers}} + [\text{EtOx}]_{6-\text{mers}} = 113.158 \times 8 + 99.13 \times 6 + 32.042 + 22.99 = 1555.08$$

$$[n\text{PrOx}]_{7-\text{mers}} + [\text{EtOx}]_{7-\text{mers}} = 113.158 \times 7 + 99.13 \times 7 + 32.042 + 22.99 = 1541.05$$

Similar results for the other three random copolymers (P*n*PrOx$_{5\%}$EtOx$_{95\%}$, P*n*PrOx$_{25\%}$EtOx$_{75\%}$, and P*n*PrOx$_{75\%}$EtOx$_{25\%}$) with different monomer ratios in the feed were also confirmed by MALDI−TOF mass spectrometry (data not shown).

Determination of the Cloud Points (T_{cp}). The measurement of a 10% decrease point in optical transmittance, defined here as the cloud points (T_{cp}), was adapted to determine the lower critical solution temperature (LCST) of a polymer solution.

Figure 11a showed the dependence of the turbidity on the increasing temperature for the (co)polymer solutions with the different compositions between *n*PrOx and *i*PrOx. The transmittance sharply decreased at a specific temperature in phosphate-buffered solution (10 mM PBS (pH = 7.4)), indicating a sharp LCST-type phase transition. The LCST values of P(*n*PrOx-*grad*-*i*PrOx) were found to linearly decrease with the increasing mole% of *n*PrOx (l), from 38.7 °C at $l = 0\%$ to 23.8 °C at $l = 100\%$ for a 1.0 wt % polymer solution (Figure 11b). Regardless of the *n*PrOx to *i*PrOx ratio, an exceedingly clear sensitivity of the phase separation was observed in all cases (Table 1). Although P(*n*PrOx-*grad*-*i*PrOx) has a compositional gradient along the copolymer strand, a notable point to emphasize about this turbidimetric result is that the observed transition behavior was appreciably sharp and simply connected to the composition ratio of both monomers in the copolymers. Of special interest was the P*n*PrOx homopolymer independently exhibiting a sharp

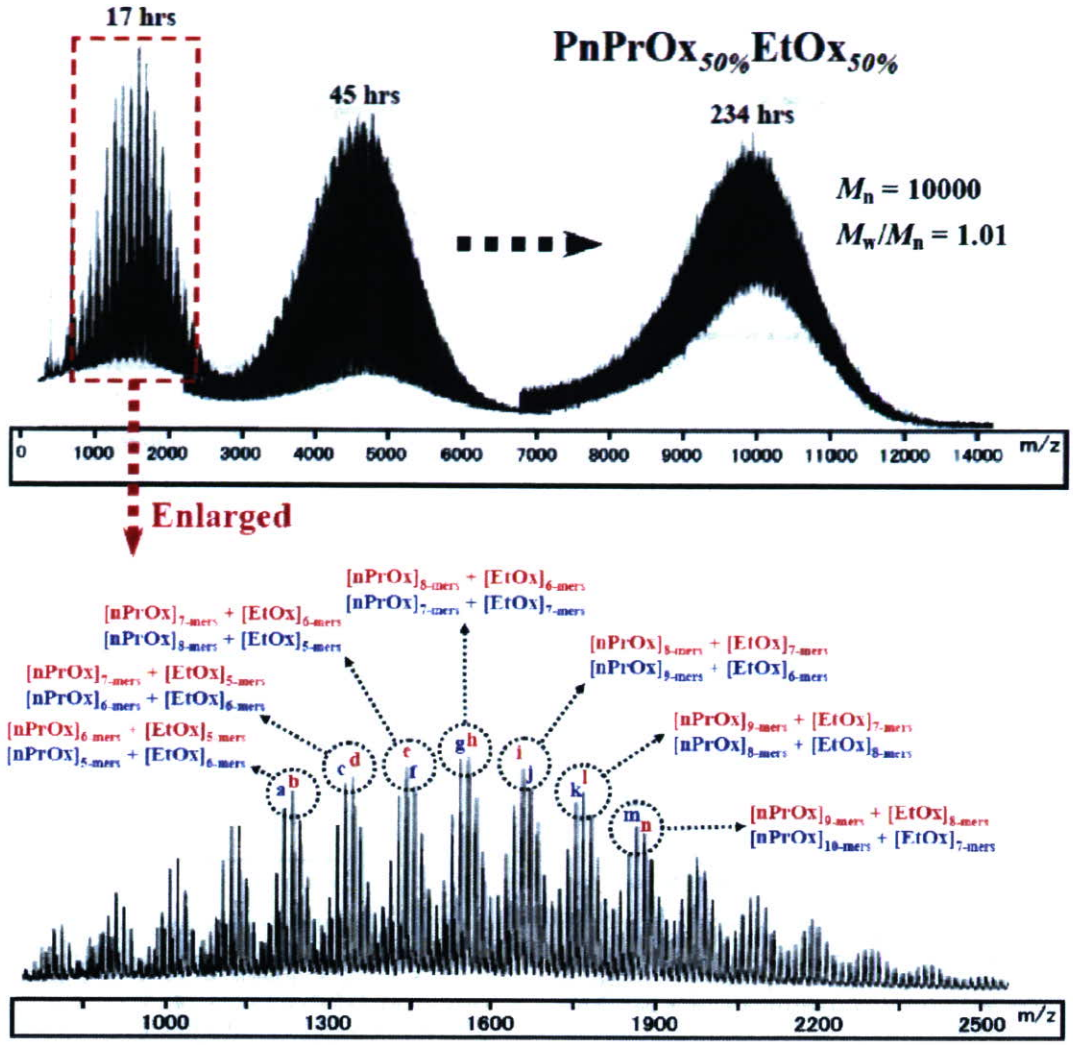

Figure 10. MALDI−TOF mass spectra of random copolymer samples comprising *n*PrOx$_{50\%}$ and EtOx$_{50\%}$ after 17, 45, and 234 h (upper), and enlarged detail in the mass region of 700−2500 for the first sampling P*n*PrOx$_{50\%}$EtOx$_{50\%}$ after 17 h (lower).

Table 3. Assignment of MALDI-TOF Mass Spectral Peaks Shown in Figure 10

$mass_{exp}$	$mass_{calc}$	assignment	$mass_{exp}$	$mass_{calc}$	assignment
1213.92	1215.60	a. $[nPrOx]_{5\text{-mers}} + [EtOx]_{6\text{-mers}}$	1227.96	1229.63	b. $[nPrOx]_{6\text{-mers}} + [EtOx]_{5\text{-mers}}$
1327.49	1328.76	c. $[nPrOx]_{6\text{-mers}} + [EtOx]_{6\text{-mers}}$	1341.52	1342.79	d. $[nPrOx]_{7\text{-mers}} + [EtOx]_{5\text{-mers}}$
1455.19	1455.95	f. $[nPrOx]_{8\text{-mers}} + [EtOx]_{5\text{-mers}}$	1440.96	1441.92	e. $[nPrOx]_{7\text{-mers}} + [EtOx]_{6\text{-mers}}$
1540.12	1541.05	g. $[nPrOx]_{7\text{-mers}} + [EtOx]_{7\text{-mers}}$	1554.36	1555.08	h. $[nPrOx]_{8\text{-mers}} + [EtOx]_{6\text{-mers}}$
1667.71	1668.23	j. $[nPrOx]_{9\text{-mers}} + [EtOx]_{6\text{-mers}}$	1653.53	1654.21	i. $[nPrOx]_{8\text{-mers}} + [EtOx]_{7\text{-mers}}$
1752.64	1753.34	k. $[nPrOx]_{8\text{-mers}} + [EtOx]_{8\text{-mers}}$	1766.76	1767.36	l. $[nPrOx]_{9\text{-mers}} + [EtOx]_{7\text{-mers}}$
1880.17	1880.522	m. $[nPrOx]_{10\text{-mers}} + [EtOx]_{7\text{-mers}}$	1865.95	1866.49	n. $[nPrOx]_{9\text{-mers}} + [EtOx]_{8\text{-mers}}$

LCST behavior near room temperature. The LCST (23.8 °C) of P*n*PrOx with a more hydrophobic 2-*n*-propyl side group was lower by a large margin compared to that (62−65 °C) of the PEtOx high polymers, but almost constant regardless of the increasing molecular weight and concentration (data not shown). In addition, the LCST of P*n*PrOx was also lower than that (38.7 °C) of P*i*PrOx, a chemical isomer of P*n*PrOx. This difference in LCST ($\Delta = 14.9$ °C) between P*n*PrOx and P*i*PrOx could be explained by the similar trend between PNiPAAm and poly(*N*-*n*-propylacrylamide) (PNnPAAm), viz., the lower LCST of PNnPAAm than PNiPAAm is ascribed to a reduced solvent accessible area of the linear *n*-propyl group against the branched isopropyl group.[20]

Similarly, Figure 12a shows the dependence of the turbidity on the increasing temperature for the (co)polymer solutions with the different compositions between *n*PrOx and EtOx. The transmittance sharply decreased at a specific temperature in phosphate-buffered solution (10 mM PBS (pH = 7.4)). The LCST values of P(*n*PrOx-*ran*-EtOx) increased linearly with decreasing the content of *n*PrOx to 32 mol % from 23.8 °C at

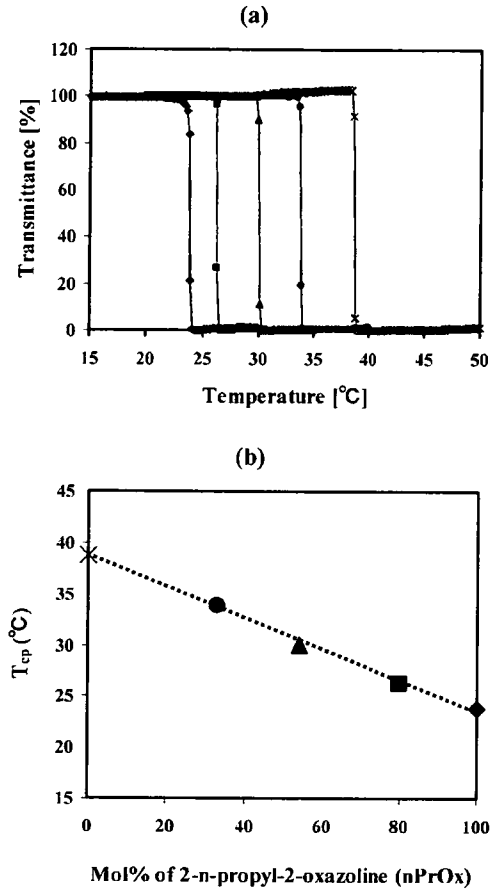

Figure 11. (a) Transmittance changes at 500 nm of 1.0 wt % gradient (co)polymer solutions (P*n*PrOx (◆), P*n*PrOx$_{25\%}$*i*PrOx$_{75\%}$ (●), P*n*PrOx$_{50\%}$*i*-PrOx$_{50\%}$ (▲), P*n*PrOx$_{75\%}$*i*PrOx$_{25\%}$ (■), and P*i*PrOx (×)) as a function of temperature (10 mM PBS (pH = 7.4); rate, 0.5 °C/min). (b) Relationship between cloud point (T_{cp}) and composition in the P(*n*PrOx-*grad*-*i*PrOx) (co)polymers.

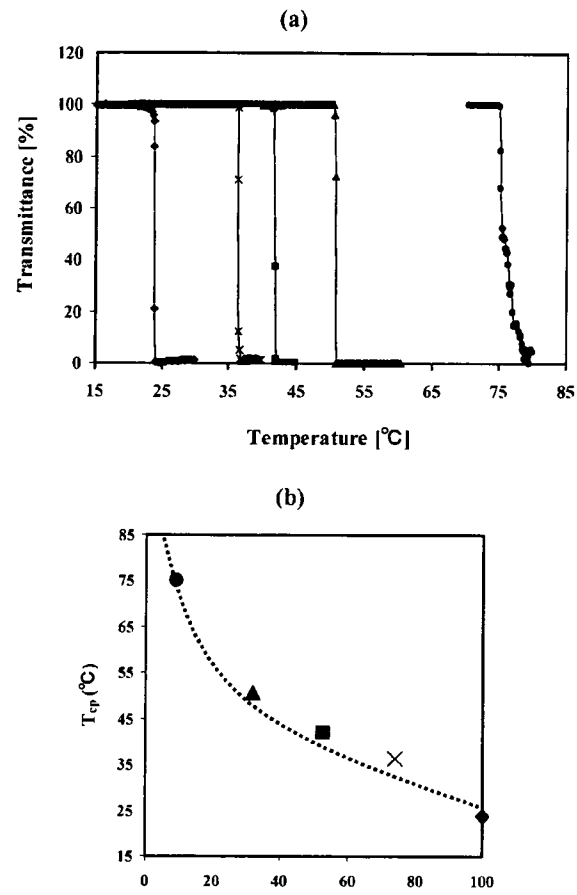

Figure 12. (a) Transmittance changes at 500 nm of 1.0 wt % random (co)polymer solutions (P*n*PrOx (◆), P*n*PrOx$_{5\%}$EtOx$_{95\%}$ (●), P*n*PrOx$_{25\%}$-EtOx$_{75\%}$ (▲), P*n*PrOx$_{50\%}$EtOx$_{50\%}$ (■), P*n*PrOx$_{75\%}$EtOx$_{25\%}$ (×)) as a function of temperature (10 mM PBS (pH = 7.4); rate, 0.5 °C/min). (b) Relationship between cloud point (T_{cp}) and composition in the P(*n*PrOx-*ran*-EtOx) (co)polymers.

I = 100% to 50.6 °C at I = 32% for a 1.0 wt % polymer solution, but progressively increased in the region below I = 32% approaching to 75.1 °C at I = 9% (Figure 12b). No observable change in the transmittance appeared in the case of a 100% PEtOx homopolymer ($M_{n,GPC}$ = 8000, $M_{n,TOF-MS}$ = 8300) as previously described.[9] Regardless of the *n*PrOx to EtOx ratio, an exceedingly clear sensitivity of the phase separation was observed with the increasing temperature in all cases (Table 2).

It may be reasonable to assume that the LCST property of such a gradient copolymer as P(*n*PrOx-*grad*-*i*PrOx) may become more complicated than P(*n*PrOx-*ran*-EtOx) with a simple random composition, due to the possible formation of a micelle-like molecular association derived from a deviating amphiphilicity along the polymer strand. Thus, P(*n*PrOx-*ran*-EtOx) could be ideal for a wide range of LCST tunings rather than P(*n*PrOx-*grad*-*i*PrOx), unless there is a specific application to target the gradient copolymer. Nevertheless, the static light scattering (SLS) measurements of P(*n*PrOx-*grad*-*i*PrOx) with varying temperatures provided no obvious evidence of the multimolecular association such as micelle structures, as in the P(*i*PrOx-*grad*-EtOx) system (data not shown). Although we may not exclude the possibility of different hydration states between the gradient and random copolymers below the LCST due to the distinct structure and composition of the two monomers incorporated in the respective copolymer strand, the turbidimetric behaviors of both copolymers followed a simple and practical rule correlated to the molar ratio of both monomers. Detailed solution behaviors of these gradient and random copolymers including the P*n*PrOx homopolymer should be an important topic for further study to understand their fundamental molecular dynamics related to temperature changes, but we recall that the present study focused on the well-defined Ox polymerization as a convenient synthetic route to selectively obtain the gradient or random copolymers with finely tuned LCSTs.

Conclusions

This study established the facile and selective synthetic route of thermosensitive POx gradient or random copolymers via the living cationic process between *n*PrOx and *i*PrOx (or EtOx). The respective monomer reactivity ratios were found to be 3.15 and 0.57 for *n*PrOx and *i*PrOx, respectively, sufficiently different to form the gradient copolymers P(*n*PrOx-*grad*-*i*PrOx), and 1.28 and 1.04 for *n*PrOx and EtOx, respectively, appropriate to obtain the random copolymers P(*n*PrOx-*ran*-EtOx). Turbidity measurements revealed that the LCST of both the gradient and random copolymers could be precisely tuned over a broad range of temperatures by varying the molar ratio of the two Ox monomers. This methodology of copolymerizing a variety of Ox monomers with different hydrophobic and hydrophilic balances, apparently lead to the systematic preparation of a series

of well-defined gradient and random POx copolymers with finely tuned LCSTs. Most of all, P(*n*PrOx-*ran*-EtOx) with a simple random sequence in the backbone showed a rapid and modulated response to the temperature change from 23.8 to 75.1 °C, considered the most ideal system for tuning the LCST around the physiological condition. These POx (co)polymers also have a promising use in biomedical applications, such as the preparation of thermosensitive bioconjugates and drug delivery systems via the synthesis of biofunctional block or graft copolymers.

Acknowledgment. This work was financially supported by the Special Coordination Funds for Science and Technology from the Ministry of Education, Culture, Sports, Science, and Technology of Japan (MEXT) as well as by the Core Research for Evolutional Science and Technology (CREST) from the Japan Science and Technology Agency (JST). The authors are also grateful to Prof. T. Tsuruta, Professor Emeritus, The University of Tokyo, for his valuable discussions and critical comments on this research.

References and Notes

(1) (a) Bergbreiter, D. E.; Osburn, P. L.; Wilson, A.; Sink, E. M. *J. Am. Chem. Soc.* **2000**, *122*, 9058. (b) Hamamoto, H.; Suzuki, Y.; Yamada, Y.; Tabata, H.; Takahashi, H.; Ikegami, S. *Angew. Chem., Int. Ed.* **2005**, *44*, 4536.

(2) (a) Uchiyama, S.; Kawai, N.; de Silva, A. P.; Iwai, K. *J. Am. Chem. Soc.* **2004**, *126*, 3032. (b) Hu, Z. B.; Chen, Y. Y.; Wang, C. J.; Zheng, Y. D.; Li, Y. *Nature*, **1998**, *393*, 149.

(3) (a) Kanazawa, H.; Yamamoto, K.; Matsushima, Y.; Takai, N.; Kikuchi, A.; Sakurai, Y.; Okano, T. *Anal. Chem.* **1996**, *68*, 100. (b) Kikuchi, A.; Okano, T. *Prog. Polym. Sci.* **2002**, *27*, 1165.

(4) (a) Stayton, P. S.; Shimoboji, T.; Long, C.; Chilkoti, A.; Chen, G.; Harris, J. M.; Hoffman, A. S. *Nature (London)* **1995**, *378*, 472. (b) Matsukata, M.; Aoki, T.; Sanui, K.; Ogata, N.; Kikuchi, A.; Sakurai, Y.; Okano, T. *Bioconjugate Chem.* **1996**, *7*, 96. (c) Ding, Z.; Chen, G.; Hoffman, A. S. *J. Biomed. Mater. Res.* **1998**, *39*, 498.

(5) (a) Yoshida, R.; Sakai, T.; Okano, T.; Sakurai, Y.; Bae, Y. H.; Kim, S. W. *J. Biomater. Sci. Polym. Ed.* **1991**, *3*, 155. (b) Cammas, S.; Suzuki, K.; Sone, Y.; Kakurai, Y.; Kataoka, K.; Okano, T. *J. Controlled Release.* **1997**, *48*, 157. (c) Kono, K. *Adv. Drug. Deliv. Rev.* **2001**, *53*, 307.

(6) (a) Park, J. S.; Akiyama, Y.; Winnik, F. M.; Kataoka, K. *Macromolecules* **2004**, *37*, 6786. (b) Diab, C.; Akiyama, Y.; Kataoka, K.; Winnik, F. M. *Macromolecules* **2004**, *37*, 2556.

(7) (a) Heskins, M.; Guillet, J. E. *J. Macromol. Sci. Chem.* **1968**, *A2*, 1441. (b) Schild, H. G. *Prog. Polym. Sci.* **1992**, *17*, 163.

(8) Park, J. S.; Akiyama, Y.; Yamasaki, Y;, Kataoka, K. *Langmuir* **2007**, *23*, 138.

(9) Park, J. S.; Kataoka, K. *Macromolecules* **2006**, *39*, 6622.

(10) (a) Kobayashi, S. *Prog. Polym. Sci.* **1990**, *15*, 751. (b) Aoi, K.; Okada, M. *Prog. Polym. Sci.* **1996**, *21*, 151. (c) Kobayashi, S.; Uyama, H. *J. Polym. Sci., Part A: Polym. Chem.* **2002**, *40*, 192.

(11) (a) Chiu, T. T.; Thill, B. P.; Fairchok, W. J. In *Water-Soluble Polymers*; Advances in Chemistry Series 213; Glass, J. E., Ed.; American Chemical Society: Washington, DC, 1986; pp 425−433. (b) Lin, P.; Pearce, E. M.; Kwei, T. K. *J. Polym. Sci., Part B: Polym. Phys.* **1988**, *26*, 603.

(12) Chujo, Y.; Sada, K.; Matsumoto, K.; Saegusa, T. *Macromolecules* **1990**, *23*, 1234.

(13) Perrin, D. D.; Armarego, W. L. F.; Perrin, D. R. *Purification of Laboratory Chemicals*; Pergamon: Oxford, U.K., 1980.

(14) (a) Levy, A.; Litt, M. *J. Polym. Sci., Part A-1* **1968**, *6*, 1883. (b) Litt, M.; Levy, A.; Herz, J. *J. Macromol. Sci., Chem.* **1975**, *A9, 703*. (c) Warakomski, J. M.; Thill, B. P. *J. Polym. Sci., Part, A.* **1990**, *28*, 3551.

(15) Hammett, L. P. *J. Am. Chem. Soc.* **1937**, *59*, 96.

(16) Tidwell, P. W.; Mortimer, G. A. *J. Macromol. Sci. Rev. Macromol. Chem.* **1970**, *C4*, 281.

(17) (a) Pakula, T.; Matyjaszewski, K. *Macromol. Theory Simul.* **1996**, *5*, 987. (b) Matyjaszewski, K.; Ziegler, M. J.; Arehart, S. V.; Greszta, D.; Pakula, T. *J. Phys. Org. Chem.* **2000**, *13*, 775. (c) Madruga, E. L. *Prog. Polym. Sci.* **2002**, *27*, 1879.

(18) Hagipol, C. *Copolymerization-Toward a Systematic Approach*; Kluwer Academic: New York, 1999.

(19) (a) Montaudo, M. S. *Rapid Commun. Mass Spectrom.* **1999**, *13*, 639. (b) Montaudo, M. S. *Mass Spectrom. Rev.* **2002**, *21*, 108.

(20) Mao, H.; Li, C.; Zhang, Y.; Furyk, S.; Cremer, P. S.; Bergbreiter, D. E. *Macromolecules* **2004**, *37*, 1031.

MA0701181

Gene Therapy (2007) 14, 1029–1038

www.nature.com/gt

ORIGINAL ARTICLE

Biocompatible micellar nanovectors achieve efficient gene transfer to vascular lesions without cytotoxicity and thrombus formation

D Akagi[1,2], M Oba[3], H Koyama[3], N Nishiyama[4], S Fukushima[2], T Miyata[1], H Nagawa[1] and K Kataoka[2,4,5]

[1]*Division of Vascular Surgery, Department of Surgery, Graduate School of Medicine, The University of Tokyo, Bunkyo-ku, Tokyo, Japan;* [2]*Department of Materials Engineering, Graduate School of Engineering, The University of Tokyo, Bunkyo-ku, Tokyo, Japan;* [3]*Department of Vascular Regeneration, Graduate School of Medicine, The University of Tokyo, Bunkyo-ku, Tokyo, Japan;* [4]*Division of Clinical Biotechnology, Center for Disease Biology and Integrative Medicine, Graduate School of Medicine, The University of Tokyo, Bunkyo-ku, Tokyo, Japan and* [5]*Center for NanoBio Integration, The University of Tokyo, Bunkyo-ku, Tokyo, Japan*

Gene therapy, a promising treatment for vascular disease, requires appropriate gene vectors with high gene transfer efficiency, good biocompatibility and low cytotoxicity. To satisfy these requirements from the approach of nonviral vectors, a novel block copolymer, poly(ethylene glycol) (PEG)-block-polycation, carrying ethylenediamine units in the side chain (PEG-b-P[Asp(DET)]) was prepared. PEG-b-P[Asp(DET)] formed a polyplex micelle through polyion complex formation with plasmid DNA (pDNA). The PEG-b-P[Asp(DET)] polyplex micelle showed efficient gene expression with low cytotoxicity against vascular smooth muscle cells in vitro. *It also showed reduced interactions with blood components, offering its feasibility of gene delivery via the vessel lumen. To evaluate* in vivo *gene transfer efficiency for vascular lesions, PEG-b-P[Asp(DET)] micelle was instilled into rabbit carotid artery with neointima by an intravascular method, and expression of the reporter gene in vascular lesions was assessed. Polyplexes from homopolymer P[Asp(DET)] and branched polyethyleneimine (BPEI) were used as controls. Ultimately, only the polyplex micelle showed appreciable gene transfer into vascular lesions without any vessel occlusion by thrombus, which was in strong contrast to BPEI and P[Asp(DET)] polyplexes which frequently showed occlusion with thrombus. These findings suggest that the PEG-b-P[Asp(DET)] polyplex micelle may have promising potential as a nonviral vector for the treatment of vascular diseases.*
Gene Therapy (2007) **14**, 1029–1038. doi:10.1038/sj.gt.3302945; published online 26 April 2007

Keywords: *gene delivery; non-viral gene vector; polyplex micelle; vascular disease; intimal hyperplasia; biocompatibility*

Introduction

Local gene delivery is a promising approach for the treatment of refractory vascular disease. Previous studies have presented a variety of strategies for transferring therapeutic genes to the vascular wall.[1,2] Viral vectors, such as adenovirus vector, have been commonly utilized in these strategies, because the gene transfer efficiency with a viral vector is generally higher than that by other nonviral methods. However, the clinical use of viral vectors has considerable limitations with respect to safety.[3,4] For therapeutic application of gene delivery to the vascular wall, it is, therefore, desirable to develop a nonviral vector with safety and reasonable efficiency of gene transfer.

Several cationic polymers (polycations), which form a polyion complex with DNA (polyplex) and then promote introduction of the DNA into cells, have been widely used as nonviral vectors in several studies *in vitro*.[5,6] However, positively charged polyplexes might potentially induce cytotoxicity and form aggregates in biological media containing plasma proteins, indicating that *in vivo* applications of such polyplexes might be markedly restricted.[7,8] To resolve this issue, we recently designed biocompatible nonviral vectors constructed from newly synthesized cationic block copolymer.[9] The block copolymer thus synthesized is characterized by tandem alignment of a hydrophilic poly(ethylene glycol) (PEG) segment and a cationic polyaspartamide segment carrying an ethylenediamine unit at the side chain (PEG-*b*-P[Asp(DET)]) (Figure 1a),[10] leading to the formation of stable and biocompatible polyplex micelles with a core of tightly packed plasmid DNA (pDNA) surrounded by a dense shell layer of PEG (Figure 1b). Because of the hydrophilicity as well as the strong steric-repulsive propensity of the PEG shell, the polyplex micelles are assumed to be stable in physiological entities including harsh *in vivo* conditions.[11] Furthermore, after internalization of the polyplex micelles into cellular compartments through the endocytic pathway, the ethylenediamine unit in the block copolymer is expected to facilitate efficient

Correspondence: Professor K Kataoka, Department of Materials Engineering, Graduate School of Engineering, The University of Tokyo, 7-3-1 Hongo, Bunkyo-ku, Tokyo 113-0033, Japan.
E-mail: kataoka@bmw.t.u-tokyo.ac.jp
Received 16 September 2006; revised 24 January 2007; accepted 31 January 2007; published online 26 April 2007

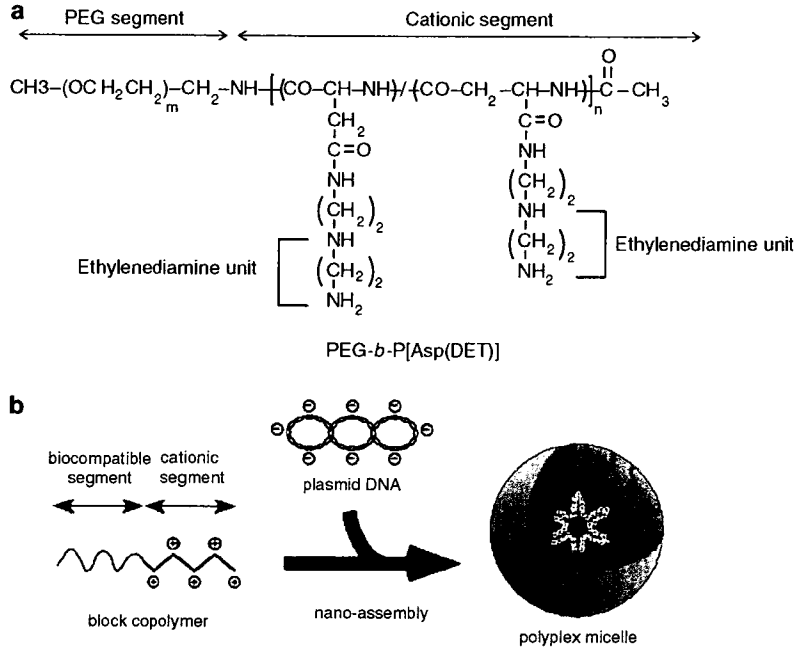

Figure 1 (a) Chemical structure of PEG-*b*-P[Asp(DET)] block copolymer. (b) Schematic illustrations of the polyplex micelle formation through electrostatic force.

translocation of the micelle toward the cytoplasm due to the proton sponge mechanism based on its high buffering capacity.[12] A previous study indeed revealed that polyplex micelles made from PEG-*b*-P[Asp(DET)] accomplished appreciably high gene transfection efficacy with remarkably low cytotoxicity toward several cultured cell lines as well as primary osteoblasts.[10]

In the present study, the utility of the polyplex micelle from PEG-*b*-P[Asp(DET)] for transfection to vascular lesions was investigated to evaluate its feasibility for vascular gene therapy. The polyplex micelle was revealed to have excellent colloidal stability even in proteinaceous medium and reduced interactions with blood components, showing appreciable gene transfection efficacy toward primary vascular smooth muscle cells (VSMC) under *in vitro* conditions. Furthermore, *in vivo* transfection of a reporter gene to rabbit carotid artery with induced neointimal lesions was successfully done, with high transfection ability and markedly reduced cytotoxicity and thrombogenicity of the polyplex micelles, making it feasible for vascular gene therapy.

Results

In vitro *gene transfer to VSMC*

The gene expression efficacy was evaluated as expressed luciferase activity. Expression pDNA containing the luciferase gene (*pCAccluc+*) was transferred to cultured VSMC using the polyplex micelle from PEG-*b*-P[Asp(DET)] to assess the gene transfection efficiency of the micelle from the activity of expressed luciferase after 48 h of culture. Polyplexes from branched polyethyleneimine (BPEI) and P[Asp(DET)] were used as controls. Note that P[Asp(DET)] is the homopolymer of Asp(DET), and was selected as a control to estimate the effect of PEG

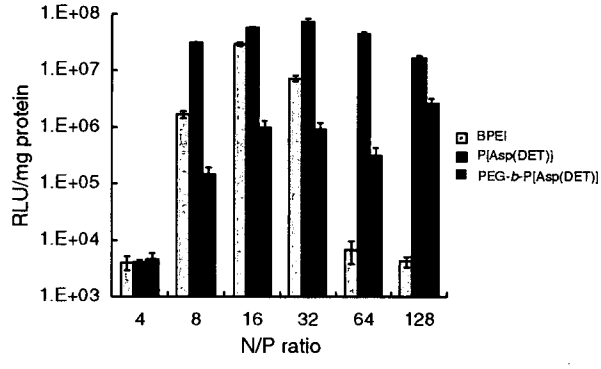

Figure 2 *In vitro* gene expression as measured by luciferase activity at 48 h after administration of BPEI polyplex, P[Asp(DET)] polyplex and PEG-*b*-P[Asp(DET)] micelle. Each polymer was complexed with pCAcc-luc+ at various N/P ratios, and applied to cultured VSMC. Forty-eight hours later, the cells were lysed, and luciferase activity of the lysates was measured. Values are expressed as RLU/mg protein. Values are shown as mean±s.e.m.

on physicochemical and biological characteristics of the polyplexes. Polyplexes of BPEI and P[Asp(DET)] as well as polyplex micelles of PEG-*b*-P[Asp(DET)] were prepared by mixing the corresponding polymer with pDNA at various N/P ratios. Here, N/P ratio refers to the unit molar ratio of the amino group in the polymer to the phosphate group in the pDNA. BPEI polyplex showed maximum transfection at an N/P ratio of 16 (Figure 2), followed by a steep decrease in efficacy, presumably due to increased cytotoxicity, as shown in Figure 3. Notably, VSMC transfected with P[Asp(DET)] polyplex and PEG-*b*-P[Asp(DET)] polyplex micelle maintained appreciably high luciferase activity at a wide range of N/P ratios >8, consistent with their lowered cytotoxicity (Figure 3). P[Asp(DET)] polyplex achieved more than tenfold higher

transfection activity than the PEG-*b*-P[Asp(DET)] micelle under this condition, and was even more effective than BPEI polyplex. It should be noted that transfection was not detectable for naked pDNA under the same conditions (data not shown).

Cytotoxicity to VSMC

Cytotoxicity to VSMC of the polyplexes and the polyplex micelles with varying N/P ratios was evaluated by MTT assay after 48 h of incubation. The viability of cells incubated with BPEI polyplex decreased linearly with an increase in N/P ratio, as seen in Figure 3. In contrast, cellular viability remained at more than 70 and 90% even after 48 h incubation with P[Asp(DET)] polyplex and PEG-*b*-P[Asp(DET)] polyplex micelle, respectively, up to an N/P ratio of 64.

Aggregate formation in albumin solution

To assess the colloidal stability of the polyplexes in biological media, they were subjected to measurements of particle size and ζ-potential after incubation for 1 h in phosphate-buffered saline (PBS) containing various concentrations of albumin. The polyplex micelle prepared at N/P = 40 maintained a size of approximately 110 nm regardless of albumin concentration, as summarized in Table 1, yet polyplexes from both BPEI (N/P = 10) and P[Asp(DET)] (N/P = 40) exhibited a marked increase in particle size in medium containing albumin at 1–2 mg/ml. The polyplexes from BPEI and P[Asp(DET)] showed highly positive ζ-potential values (~26 mV) in the absence of albumin, whereas their ζ-potential values decreased toward a neutral value with an increase in albumin concentration, presumably due to the association with anionically charged albumin molecules (Figure 4). This nonspecific association with albumin is likely to be the reason for the aggregate formation of the polyplex system in the presence of albumin observed in Table 1. In contrast, the polyplex micelle had an almost neutral ζ-potential with a small absolute value over a wide range of albumin concentrations (Figure 4), indicating improved colloidal stability of the polyplex micelle compared to conventional polyplexes with a cationic nature.

Measurement of platelet aggregation using platelet-rich plasma

It is known that platelet aggregation plays a pivotal role in the initial stage of the thrombus formation. To estimate the thrombogenicity of the polyplexes and micelles, they were mixed with platelet-rich plasma (PRP), and the platelet aggregation was evaluated by a laser-scattering aggregometer PA-200 (Kowa, Tokyo, Japan). In this measurement, aggregate formation was measured as an increase in the light-scattering intensity (LSI; in mV). The size of detected aggregates was tentatively defined by LSI and was classified as 'small', 'medium' and 'large' as

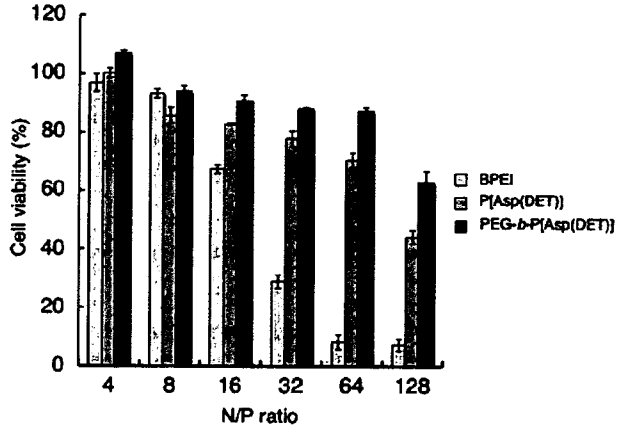

Figure 3 *In vitro* cytotoxicity to VSMC after 48 h incubation with BPEI polyplex, P[Asp(DET)] polyplex and PEG-*b*-P[Asp(DET)] micelle. Each polymer was complexed with pDNA at various N/P ratios, and applied to cultured VSMC ($n = 4$, each). Forty-eight hours later, cell viability was assessed by MTT assay. Values are shown as mean ± s.e.m.

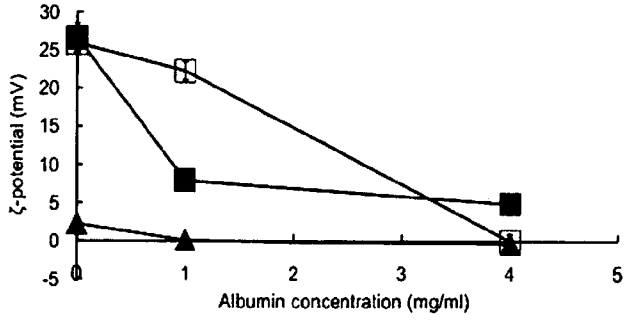

Figure 4 ζ-potential of BPEI polyplex (N/P = 10) (open squares), P[Asp(DET)] (N/P = 40) (solid squares), and PEG-*b*-P[Asp(DET)] micelle (N/P ratio = 40) (triangles) in the medium containing varying concentrations of albumin solution ($n = 3$). Values are shown as mean ± s.e.m.

Table 1 Particle size analysis in the medium with varying albumin concentrations (nm)

	Albumin concentration (mg/ml)					
	0	*0.01*	*0.1*	*1*	*2*	*4*
BPEI polyplex	136.3	130.0	131.3	141.7	ND[a]	ND[a]
P[Asp(DET)] polyplex	141.7	120.3	167.3	ND[a]	ND[a]	ND[a]
PEG-*b*-P[Asp(DET)] micelle	112.0	108.7	117.7	111.3	112.7	111.7

Abbreviations: BPEI, branched polyethyleneimine; ND, not determined; PEG, poly(ethylene glycol).
BPEI N/P = 10, P[Asp(DET)] N/P = 40, PEG-*b*-P[Asp(DET)] N/P = 40.
[a]Not determined because of aggregate formation.

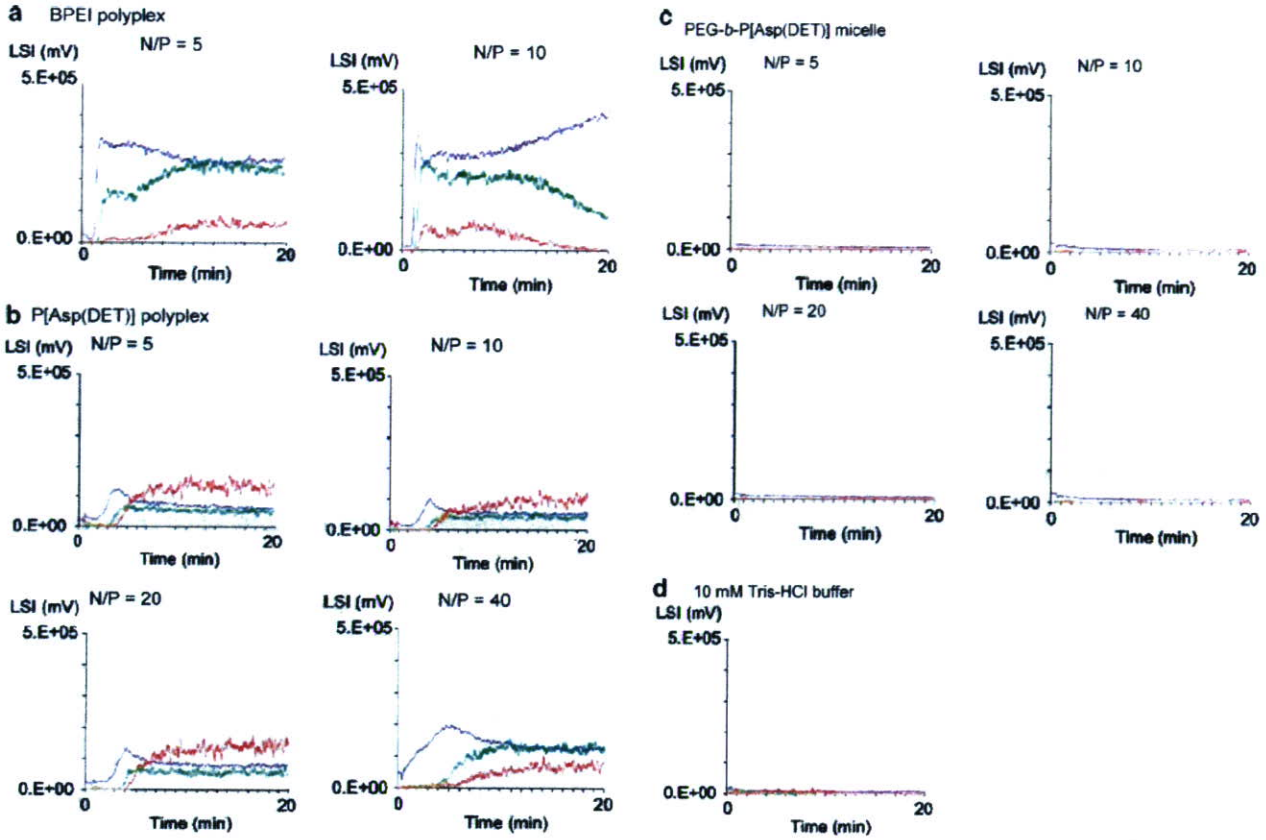

Figure 5 Time-dependent profiles of platelet aggregation by a laser-scattering aggregometer PA-200 after mixing PRP (240 μl) with the polyplexes (60 μl) or the micelles (60 μl); (**a**) BPEI polyplexes (N/P = 5, 10); (**b**) P[Asp(DET) polyplexes (N/P = 5, 10, 20, 40); (**c**) PEG-*b*-P[Asp(DET)] micelle (N/P = 5, 10, 20, 40) and (**d**) 10 mM Tris-HCl buffer (pH 7.4). The vertical values are expressed as the LSI, the unit of which is milli volts (mV). In each figure, the blue, green and red profiles correspond to the aggregates classified as 'small', 'medium' and 'large' (see Materials and methods section), respectively (Min, minute).

described in the Materials and methods section. BPEI and P[Asp(DET)] polyplexes showed an appreciable increase in the LSI of 'small', 'medium' and 'large' category at any N/P ratios (Figure 5a and b), suggesting the significant platelet aggregation. In contrast, PEG-*b*-P[Asp(DET)] micelle showed no increase in the LSI at any N/P ratios (Figure 5c and d), indicating that the PEG shell of the polyplex micelles effectively prevented the aggregation of platelets.

Erythrocyte aggregation assay

To further study the interaction between the polyplexes and blood cells, erythrocyte aggregation assay was carried out. It is known that erythrocytes possess negative surface charge and interact with positively charged nano-particles, resulting in the aggregate formation.[13] Erythrocytes were harvested from blood of rabbit, followed by washing and suspension with Ringer's solution to avoid the effect of serum proteins. Figure 6 revealed that erythrocytes incubated with BPEI (Figure 6a) and P[Asp(DET)] polyplexes (Figure 6b) underwent aggregation regardless of N/P ratios. By contrast, erythrocytes incubated with PEG-*b*-P[Asp(DET)] micelle did not undergo any aggregation (Figure 6c), keeping the dispersivity comparable to those in 10 mM Tris-HCl buffer (Figure 6d). These results clearly indicate that neutral and sterically repulsive properties of the polyplex micelle might also effectively prevent the erythrocyte aggregation through the electrostatic interaction.

Gene transfer to injured rabbit carotid artery

Rabbit carotid artery was injured with a Fogarty balloon catheter to induce neointimal hyperplasia. Twenty-one days later, BPEI (N/P = 10) polyplex, P[Asp(DET)] (N/P = 40) polyplex, and PEG-*b*-P[Asp(DET)] (N/P = 40) micelle were administered into the carotid artery with neointimal involvement and incubated by cessation of arterial blood flow for 20 min. N/P ratios of the polyplexes and micelles used for *in vivo* experiments were adjusted to the appropriate values based on the results of *in vitro* experiments, that is, the balance between the cytotoxicity (Figure 3) and the transfection efficiency (Figure 2). Note that the aggregation assay using albumin (Table 1 and Figure 4), platelets (Figure 5) and erythrocytes (Figure 6) revealed that PEG-*b*-P[Asp(DET)] micelle had minimal interaction with these biocomponents at any N/P ratios. The entrapped pDNA in the polyplex and the micelle was the expression plasmid vector containing the luciferase gene (*pCAccluc+*). Naked pDNA (*pCAccluc+*) was applied in the same manner as controls. At 3 days after the treatment, the carotid arteries were sampled to assess luciferase activity in each layer of the arterial wall (Figure 7a). All of the rabbits that received naked pDNA ($n = 8$) or the polyplex micelle ($n = 8$) had 100% patency of the carotid artery, whereas considerable

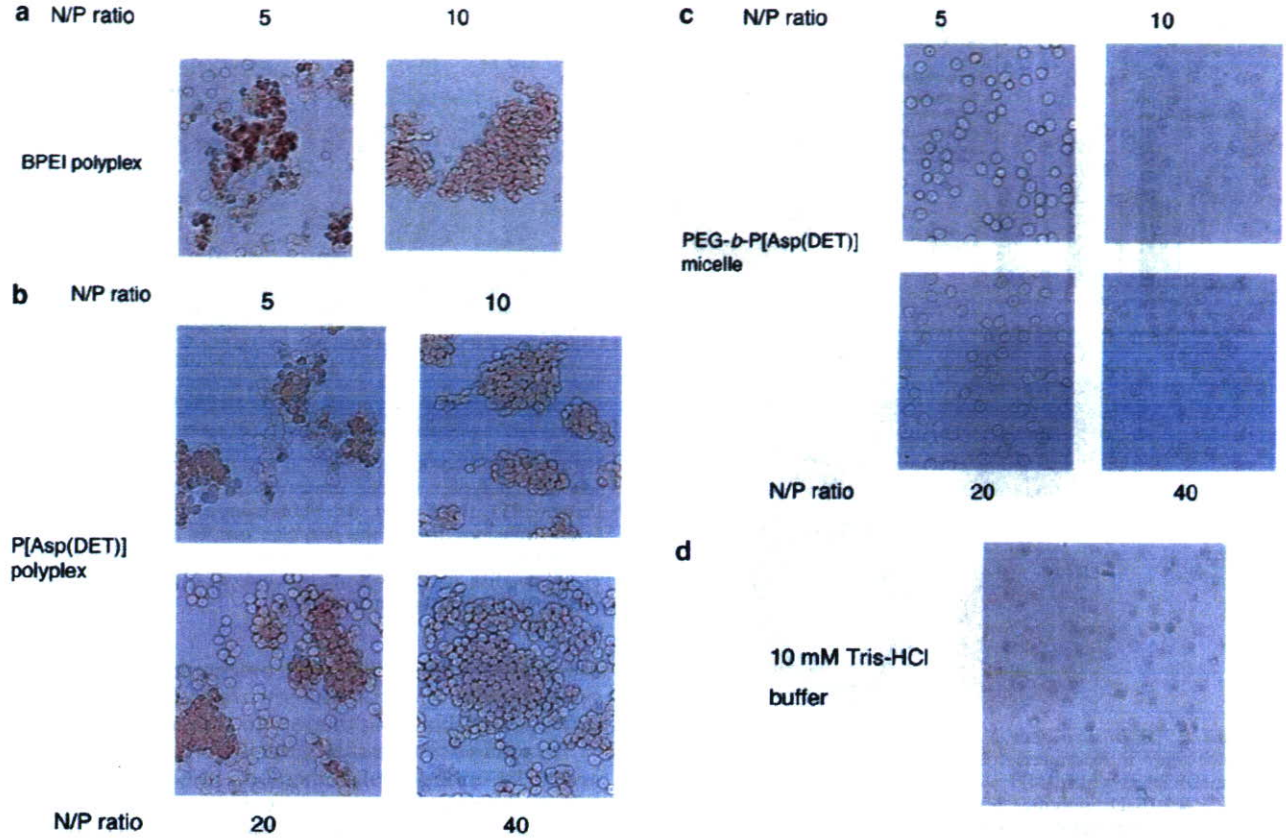

Figure 6 Photomicrographs of erythrocytes mixed and incubated for 1 h at 37°C with or without polyplexes varying N/P ratios: (**a**) BPEI polyplex (N/P = 5 and 10); (**b**) P[Asp(DET)] polyplex (N/P = 5, 10, 20 and 40); (**c**) PEG-*b*-P[Asp(DET)] micelle (N/P = 5, 10, 20 and 40) and (**d**) control in 10 mM Tris-HCl buffer without any polyplexes (control). Aggregation was observed in the medium containing BPEI and P[Asp(DET)] polyplex regardless of N/P ratios, although no aggregation was observed in the medium with PEG-*b*-P[Asp(DET)] micelle of varying N/P ratio.

thrombo-occlusion of the artery occurred in rabbits in which BPEI (3 occlusions in 8 samples) and P[Asp(DET)] (4 occlusions in 8 samples) polyplexes were applied. The cross sections of the patent and occluded arteries with hematoxylin-eosin stain were shown in Figure 7b–f. The lumens of the occluded arteries challenged with P[Asp(DET)] and BPEI polyplexes were filled with thrombus. All the samples subjected to BPEI polyplex, P[Asp(DET)] polyplex, and PEG-*b*-P[Asp(DET)] polyplex micelles showed significantly higher luciferase activity in the neointima, media and adventitia than those with naked pDNA. There was no significant difference in the luciferase activity among the samples with BPEI, P[Asp(DET)] and PEG-*b*-P[Asp(DET)] treatment (Figure 7a).

To confirm *in vivo* gene transfer to the arterial wall, the expression pDNA containing the FLAG sequence (*pMP-FLAG*) was then complexed with PEG-*b*-P[Asp(DET)] and administered to the carotid artery in the same manner. The artery was harvested on day 3, and a cross section of the artery was stained with anti-FLAG antibody. The immunostain clearly showed abundant FLAG-positive cells in the arterial wall, in which FLAG expression was predominantly observed in the neointima (Figure 8a). The pDNA expressing LacZ gene (*pCAZ3*) was then complexed with PEG-*b*-P[Asp(DET)] and administered to the carotid artery in the same manner as negative control. Eventually, the immunostain with anti-FLAG antibody showed no FLAG-positive cells (Figure 8b) in the control specimen.

Discussion

Vascular lesions as feasible targets for gene therapy are generally related to atherosclerosis or its associated diseases. As such lesions develop from the intimal layer of the vascular wall, the intima is a primary target of vascular gene therapy, indicating that delivery via the vessel lumen is the most appropriate approach for efficient gene transfer to vascular lesions. Fortunately, it is easy to approach the luminal surface using a catheter-based method, and several endovascular devices have been developed for this purpose in previous studies. In the vessel lumen, however, attention must be paid to interactions between the gene vector and blood components such as plasma proteins and blood cells. In particular, platelet activation and aggregation promote the coagulant and fibrinolytic pathways through activation of coagulation factors accompanying aggregation of blood cells, resulting in thrombus formation. Most nonviral gene vectors possess a positively charged component in their structure to form a complex with DNA. As blood components ordinarily carry a negative

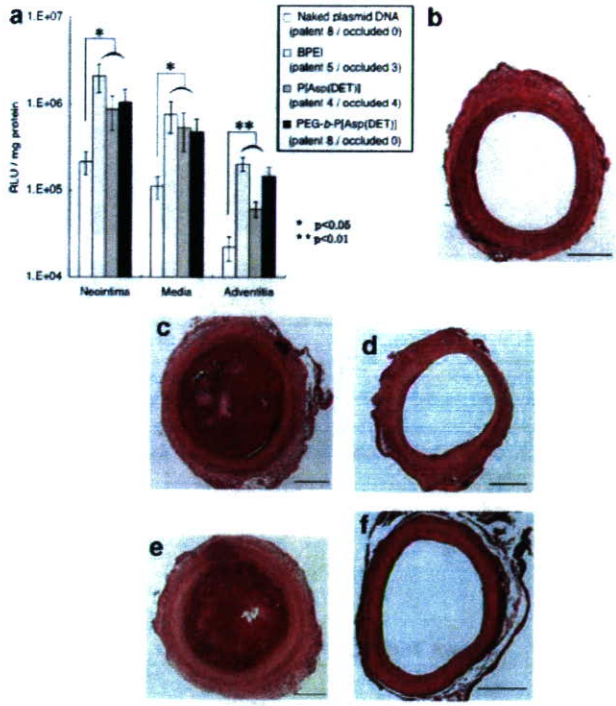

Figure 7 (**a**) *In vivo* gene expression evaluated from luciferase activity after intra-arterial delivery of BPEI polyplex (N/P = 10), P[Asp(DET)] polyplex (N/P = 40), and PEG-*b*-P[Asp(DET)] micelle (N/P = 40). Each polymer was complexed with *pCAccluc*+ and instilled into the rabbit common carotid artery with neointima. One group of animals was treated with naked pDNA (*pCAccluc*+) as control. At 72 h, the common carotid artery was excised and luciferase activity was measured. Values are expressed as RLU/mg protein. Values are shown as mean ± s.e.m. (*$P < 0.01$, **$P < 0.05$). (**b–f**) Cross sections of the gene-transferred arteries with hematoxylin-eosin stain, (**b**) patent, (**c**) occluded samples of BPEI polyplexes (N/P = 10), (**d**) patent, (**e**) occluded samples of P[Asp(DET)] polyplexes (N/P = 40) and (**f**) patent sample of PEG-*b*-P[Asp(DET)] micelle (N/P = 40). Bar = 500 μm.

charge, there is a possibility for a nonviral vector to undergo aggregation with plasma proteins and blood cells.[5,13–16] Such aggregation around a gene vector might interfere with the process of gene transfer and also induce thrombus formation, which could worsen the clinical status of the primary disease. Additionally, the positive charge of the gene vector would potentially promote cytotoxic reactions in the lesion and its surrounding part of the vascular wall. As the intima is the most accessible part in vascular gene therapy, as described, the toxic side effects derived from constituent polycations of polyplexes also predominantly appear in the intimal layer of the arterial wall, which might imply injury of intimal cells. In previous studies investigating the mechanisms of atherogenesis, various evidence has been presented to demonstrate that vascular injury is a potent trigger for lesion formation.[17,18] Injury to the vascular wall possibly promotes a variety of responses, such as expression of adhesive molecules and receptors on vascular cells, release of several growth factors, platelet adhesion on the luminal surface and infiltration of inflammatory cells.[19] These responses might influence each other, and potentially induce the formation of neointimal hyperplasia and atherosclerotic lesions. Thus,

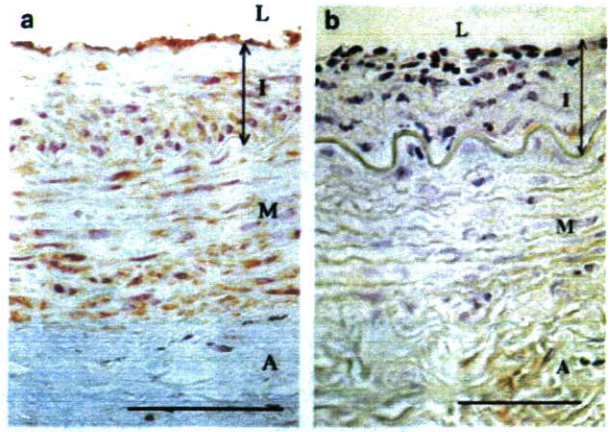

Figure 8 (**a**) Photomicrographs of rabbit carotid artery transfected with the polyplex micelle composed of pMP-FLAG and PEG-*b*-P[Asp(DET)] (N/P = 40). (**b**) Photomicrographs of rabbit carotid artery transfected with the polyplex micelle composed of pDNA expressing LacZ and PEG-*b*-P[Asp(DET)] (N/P = 40) as control. FLAG-positive region was stained brown. L, lumen; I, intima; M, media; A, adventitia. Bar = 100 μm.

minimal vascular injury with biocompatible gene vector systems with low cytotoxicity should be achieved for safe and reliable gene therapy in vascular diseases.

To achieve successful gene delivery to the carotid artery by intravascular method, polyplex micelles, in which the polyplex core is covered with PEG palisades, were used in this study. One of the advantageous characteristics of polyplex micelles with a PEG shell layer is high colloidal stability in a physiological proteinaceous medium, showing reduced interactions with blood components. It was reported that the thrombus formation are caused by nonspecific interaction between blood components and cationic materials such as polyplexes and prosthesis for intravascular application.[13–16,20–24] Srinivasan *et al*.[20] reported that positively charged prosthetic materials are highly thrombogenic. PEG is the well-known materials with hydrophilic character showing the high biocompatibility and the low thrombogenicity.[25–27] There are previous reports that the surface modification of biomaterials with PEG appreciably reduces thrombogenicity.[25,28–32] Thus, it is widely accepted that PEG shields the cationic surface of biomaterials, reducing their thrombogenicity.[31] In this study, the PEG-*b*-P[Asp(DET)] micelle system showed no agglomeration even in the presence of blood components including serum albumin (Table 1 and Figure 4), platelets (Figure 5) and erythrocytes (Figure 6), whereas BPEI and P[Asp(DET)] polyplexes definitely showed the aggregate formation due to their positively charged character under the same conditions. It should be noted that PEG-*b*-P[Asp(DET)] micelle showed no platelet and erythrocyte aggregation even at a high N/P ratios, whereas P[Asp(DET)] and BPEI polyplexes induced platelet and erythrocyte aggregation even at low N/P ratios, such as 5. These results suggest that the surface modification of polyplexes with PEG might prevent their interaction with blood components even at a high N/P ratio required for the effective gene transfection. In addition to the colloidal stability of nonviral vectors with reduced interactions with blood components, another critical issue is the incidence of cytotoxic reactions.

In this regard, the lower cytotoxicity of PEG-*b*-P[Asp(DET)] as compared to BPEI against VSMC, a primary target of vascular gene therapy of atherosclerosis, was demonstrated in Figure 3. Such reduced nonspecific interactions with blood components and low cytotoxicity of polyplex micelles should be the remarkable advantages as the system utilized for *in vivo* nonviral gene delivery via the vascular lumen. Indeed, an *in vivo* study using rabbit carotid artery revealed no occlusion after intraluminal delivery of the polyplex micelle made from PEG-*b*-P[Asp(DET)], whereas the use of polyplexes from BPEI and P[Asp(DET)] resulted in the considerable thrombo-occlusion (Figure 7).

The efficiency of *in vivo* gene transfer is the most important issue in the development of gene vectors for vascular diseases, and the choice of experimental model is crucial for obtaining proper evidence of vascular gene transfer. Experimental studies commonly employ small mammals as animal models, and the artery of such small animals preserves its normal structure even in the adult. In these arteries, because the intima consists of an endothelial monolayer, gene vectors might mainly distribute to the endothelium and medial SMC after administration via the vessel lumen. However, the intimal lesion is the principal target in most vascular gene therapy, and the major cell components of the lesion are intimal SMC and macrophages.[33] Previous studies using an arterial injury model have demonstrated several biological differences between medial SMC and intimal SMC.[33] Also in gene delivery, Guzman *et al.*[34] showed that adenovirus-mediated gene transfer to intimal SMC was highly efficient as compared with that to medial SMC. These findings suggest that the evaluation of vascular gene transfer must be carried out on diseased artery, not normal artery. In the present study, we first induced neointimal hyperplasia in the rabbit carotid artery, and then applied gene vectors to the same artery, which mimicked vascular gene delivery in the clinical setting. Because of the proper preparation of the model, it is expected to provide highly reliable data. In this study, the evaluation using this model showed that gene delivery with the BPEI, P[Asp(DET)], and PEG-*b*-P[Asp(DET)] systems all promoted marked expression of the transferred gene in the neointima, media and adventitia, which was significantly greater than that after the treatment with naked pDNA. In these findings, an interesting feature is that the *in vivo* gene expression level after PEG-*b*-P[Asp(DET)] micelle treatment was similar to that after BPEI or P[Asp(DET)] polyplex treatment (Figure 7a), although the *in vitro* transfection efficiency of the PEG-*b*-P[Asp(DET)] micelle was lower than that of BPEI and P[Asp(DET)] polyplexes (Figure 2). Histological analyses also revealed abundant expression of the marker gene in the arterial wall treated with PEG-*b*-P[Asp(DET)] micelle (Figure 8a), supporting high *in vivo* transfection ability of PEG-*b*-P[Asp(DET)] micelle to vascular lesions. The most likely explanation for such efficient gene transfer to vascular lesions *in vivo* might be an effective buffering action of PEG-*b*-P[Asp(DET)] in the acidic endosomal compartment as described previously.[10]

In conclusion, polyplex micelles from PEG-*b*-P[Asp(DET)] showed excellent colloidal stability with reduced nonspecific interactions with blood components and had a unique feature of the lowered *in vitro* cytotoxicity compared to the conventional polyplexes prepared from BPEI. They achieved efficient gene transfer to the rabbit carotid artery with neointimal hyperplasia without any vascular occlusion, whereas intraluminal delivery of BPEI and P[Asp(DET)] polyplexes induced thrombus formation. Note that the polymerization degree of the polycation segment in the block copolymer is one of the determining factors for the physicochemical property of the polyplex micelles. Block copolymers with relatively shorter polycation segments are not able to form stable polypexes,[35] whereas an increase in the polymerization degree of the polycation segment results in the decreased density of PEG palisades to impair the shielding effect. In this regard, P[Asp(DET)] segment with the polymerization degree of 68 was adopted in this study to construct the block copolymer used in the polyplex micelles, balancing the core stability mainly controlled by the polycation length and the high dispersivity in biological entity correlating mainly with the density of PEG palisades. Eventually, nonspecific interactions with blood components (Table 1, Figures 5 and 6) were effectively shielded, preventing thrombus formation, although achieving appreciable gene transfection, after the intravascular administration (Figure 7). Although there is still an issue of tuning the length of both PEG and P[Asp(DET)] segments in the block copolymer to further optimize the gene transfection and blood compatibility, the concept of the polyplex micelles with the polycation core of low toxicity and high buffering capacity surrounded by the dense PEG palisade was demonstrated to be feasible as nonviral gene vectors useful in the vascular gene therapy.

Materials and methods

Synthesis of block copolymer and homopolymer

The PEG-*b*-P[Asp(DET)] block copolymer (PEG; Mw = 12 000 g/mol, polymerization degree of P[Asp(DET)]; 68) was prepared as described previously.[10] P[Asp(DET)] was synthesized from poly(β-benzyl L-aspartate) (PBLA) by modifying the synthetic method of PEG-P[Asp(DET)]. Briefly, β-benzyl-L-aspartate *N*-carboxyanhydride was polymerized in *N,N*-dimethylformamide (DMF)/dichloromethane (1:10) at 40°C by initiation from the primary amino group of *n*-butylamine, followed by acetylation of the *N* terminus to obtain PBLA. A unimodal molecular weight distribution (*Mw/Mn* 1.20) of PBLA was confirmed by gel permeation chromatography (columns: TSK-gel G4000HHR+G3000HHR, eluent: DMF+10 mM LiCl, $T = 40$°C, detector: refractive index). The degree of polymerization of PBLA was calculated as 98 from the ^{1}H NMR spectrum (data not shown). Then, the side-chain aminolysis reaction of PBLA was performed by mixing with a 50-fold excess of diethylenetriamine in DMF at 40°C to obtain P[Asp(DET)]. DMF, dichloromethane, and acetic anhydride were purchased from Wako Pure Chemical Industries (Osaka, Japan).

Plasmids

Plasmid *pCAccluc+* was constructed by inserting the recombinant luciferase gene (luc+) into the pCAGGS expression vector. *pCAccluc+* was utilized for all experiments in the present study except morphological

evaluation. Meanwhile, plasmid *pME-FLAG* was constructed by inserting the FLAG tag sequence into the pME expression vector, and used for morphological assessment by immunohistochemical staining. Plasmid *pCAZ3* was constructed by inserting *Escherichia coli* LacZ cDNA into the pCGGGS expression vector. Plasmids were grown in *E. coli* JM109 and purified using Qiagen EndoFree Mega Kits (Qiagen, Hilden, Germany). pDNA was dissolved separately in 10 mM Tris-HCl buffer (pH 7.4), to be 375 μg/ml.

Preparation of polyplex micelle and other polyplexes

Given amounts of PEG-*b*-P[Asp(DET)], P[Asp(DET)] and BPEI were dissolved in Tris-HCl buffer (10 mM, pH 7.40) separately. The concentrations of polymers, PEG-*b*-P[Asp(DET)], P[Asp(DET)] and BPEI were 40, 20 and 5 mg/ml respectively. The polymer solution of PEG-*b*-P[Asp(DET)] was added at varying concentrations and mixed to a 2-fold excess volume of pDNA solution to form polyplex micelles at various N/P ratios. Polyplex micelles were kept overnight before being subjected to evaluation. Polymer with P[Asp(DET)] or BPEI (Mw = 25 kD, Sigma Chemical, MO, USA) was also mixed with pDNA at various N/P ratios to form polyplex. Each polyplex was subjected to evaluation 30 min after mixing.

In vitro *gene transfer to VSMC*

Human VSMC (Applied Cell Biology Research Institute, WA, USA) were seeded on 24-well culture plates and cultured in 500 μl CS-C medium (Applied Cell Biology) containing 10% serum. When the cells were in a semi-confluent condition, a solution of polyplexes (BPEI and P[Asp(DET)]) or polyplex micelle (PEG-*b*-P[Asp(DET)]) was added to each well (1 μg pDNA/well) ($n = 4$, each). After 24 h of incubation, the cells were washed with PBS and incubated additionally in CS-C for 24 h. N/P ratios of the polyplexes and the micelle were adjusted to 4, 8, 16, 32, 64 and 128. The cells were lysed in 100 μl cell culture lysis reagent (Promega, WI, USA), and luciferase activity of each lysate was quantified using a Luciferase Assay Kit (Promega). The results were expressed as relative light units (RLU) per milligram of total protein measured by bicinchoninic acid assay (Pierce, IL, USA). The experiment was repeated three times.

Cytotoxicity to VSMC

VSMC were seeded into 96-well plates and cultured in 100 μl CS-C. When the cells reached a semi-confluent condition, the polyplexes (BPEI and P[Asp(DET)]) or the micelle (PEG-*b*-P[Asp(DET)]) at various N/P ratios was added to each well (0.25 μg DNA/well) ($n = 4$, each). After 24 h of incubation, the cells were washed, and cultured in CS-C for an additional 24 h. Subsequently, cell viability in each well was evaluated using MTT assay reagent (Dojindo, Kumamoto, Japan) according to manufacturer's instructions. The experiment was repeated three times.

Dynamic light-scattering and laser-Doppler electrophoresis measurements

In dynamic light-scattering (DLS) measurement, the polyplexes, BPEI (N/P = 10) and P[Asp(DET)] (N/P = 40), or the micelle, PEG-*b*-P[Asp(DET)] (N/P = 40), were diluted in 10 mM Tris-HCl buffer (pH 7.4) to adjust the concentration of pDNA to 33.3 μg/ml ($n = 3$, each). DLS measurement was then carried out at 25 ± 0.2°C using a Zetasizer Nano ZEN3600 (Malvern Instruments, Worcestershire, UK) with a vertically polarized incident beam of 488 nm from an Ar ion laser. The scattering angle was fixed at 173°. The data were analyzed by a cumulative method to obtain the hydrodynamic diameter.

Laser-Doppler electrophoresis measurements were performed at 25 ± 0.2°C using a Zetasizer Nano equipped with a He–Ne ion laser (633 nm), and the scattering angle was set at 17° ($n = 3$, each). From the electrophoretic mobility (η), the ζ-potential was calculated using the Smoluchowski equation as follows: $\zeta = 4\pi\eta\upsilon/\varepsilon$, where υ is the viscosity and ε the dielectric constant of the solvent. The experiment was performed twice.

Measurement of platelet aggregation

Fresh blood from Japanese white rabbits (weight, 2.5–3.0 kg; Saitama Rabbitary, Saitama, Japan) was collected and immediately mixed with a 1:9 volume of 3.8% sodium citrate solution. PRP was isolated by centrifugation at the speed of 900 rounds per minute for 11 min at room temperature and collected as the supernatant. BPEI polyplexes (N/P = 5, 10), P[Asp(DET)] polyplexes (N/P = 5, 10, 20 and 40) and PEG-*b*-P[Asp(DET)] micelles (N/P = 5, 10, 20 and 40) were diluted in 10 mM Tris-HCl buffer (pH 7.4) to adjust the concentration of pDNA to 200 μg/ml. As a negative control, PRP in 10 mM Tris-HCl buffer (pH 7.4) without polyplexes were also used.

Aggregation of platelets in PRP with polyplexes or micelles was evaluated by a laser-scattering aggregometer PA-200 (Kowa). This instrument was reported to sensitively detect small aggregates consisting of only dozens of platelets formed under weak agonists.[36–39] The LSI was measured with the PA-200 to evaluate the existence and the extent of aggregates. According to the default configuration of the PA-200, the LSI was categorized to 'small', 'medium' and 'large' corresponding, respectively, to the small aggregates (9–25 μm), medium aggregates (26–50 μm) and large aggregates (51–70 μm). The results were recorded on a two-dimensional graph showing the time-dependent changes in the LSI. These experiments were repeated three times, and the representative data were shown as the results.

Erythrocyte aggregation assay

Fresh blood from Japanese white rabbits (weight, 2.5–3.0 kg; Saitama Rabbitary) was collected and immediately mixed with 20 μl heparin sodium. Erythrocytes were washed three times and suspended in Ringer's solution. Washed erythrocyte suspension (800 μl) was mixed with polyplex solution (400 μl) and incubated for 1 h at 37°C. BPEI polyplexes (N/P = 5 and 10), P[Asp(DET)] polyplexes (N/P = 5, 10, 20 and 40) and PEG-*b*-P[Asp(DET)] micelles (N/P = 5, 10, 20 and 40) were subjected to the measurement. They were all diluted in 10 mM Tris-HCl buffer (pH 7.4) to adjust the concentration of pDNA to 200 μg/ml. As a negative control, erythrocytes in 10 mM Tris-HCl buffer (pH 7.4) without polyplexes were also prepared. Aggregation of erythrocytes was evaluated under the optical microscope (Olympus, Tokyo, Japan).

Animal model and evaluation of gene transfer efficiency

All animal experiments conformed to the Guide for Care and Use of Laboratory Animals by the US National Institutes of Health (NIH Publication No. 85–23, revised 1996). Japanese white rabbits (weight, 2.5–3.0 kg; Saitama Rabbitary) fed a normal diet were anesthetized by intramuscular injection of xylazine (2.5 mg/kg) and ketamine (50 mg/kg). A 2 Fr Fogarty balloon catheter (Baxter Healthcare, CA, USA) was introduced through the first branch of the left external carotid artery and passed into the left common carotid artery. The balloon was inflated at physiological pressure and passed through the common carotid artery three times with constant rotation. At 21 days after balloon injury, proximal sites of the common carotid artery and internal carotid artery were clamped, and the left common carotid artery was filled with the polyplexes, BPEI (N/P = 10) and P[Asp(DET)] (N/P = 40), or the micelle, PEG-*b*-P[Asp(DET)] (N/P = 40), through the external carotid artery. In all experiments, each common carotid artery received 400 μl pDNA containing solution (200 μg/ml, 80 μg pDNA). After 20 min incubation, the vector solution was flushed out for washing, and then the arterial circulation was restored. As control, one group of rabbits was treated with naked pDNA (80 μg pCAccluc+) solution in the same manner. Three days later, animals were sacrificed. Evans blue (1 ml of 5% solution) was injected intravenously to mark the neointimal layer of the artery 10 min before sacrificing the animals. Then the left common carotid artery was excised and the connective tissue around the excised artery was removed, and the artery was opened longitudinally. Under a stereomicroscope, blue-stained neointima was first isolated from the artery, and then the elastic medial layer was separated from the adventitia. Each obtained sample was homogenized and lysed in 200 μl cell culture lysis reagent, and luciferase activity of each lysate was measured as described. Gene transfer efficiency was presented as the ratio of luciferase activity to the protein content. The results were expressed as RLU/mgtotal protein.

Immunohistochemical study

To evaluate the distribution of gene expression after gene transfer with PEG-*b*-P[Asp(DET)] micelles, pME-FLAG was complexed with PEG-*b*-P[Asp(DET)] (N/P = 40) and applied to rabbit carotid artery in the same manner. Three days after gene delivery, rabbits were sacrificed and subjected to perfusion fixation with 4% phosphate buffered paraformaldehyde (0.1 mol/l PO_4 buffer, pH 7.3). The carotid arteries were excised and embedded in paraffin. Cross sections (4 μm) were immunostained with a monoclonal antibody against FLAG tag (1:100, Sigma), as described previously. As a negative control, the cross sections, where PEG-*b*-P[Asp(DET)] (N/P = 40) micelle with LacZ gene (pCAZ3) was instilled, were stained with anti-FLAG tag antibody.

Statistical analysis

All values are shown as mean $\pm$ s.e.m. of biological experiments. The data of *in vivo* luciferase activity were shown as RLU/mg protein, analyzed by unpaired Student's *t*-test and considered significant at $P < 0.05$.

Acknowledgements

This work was supported by The Special Coordination Funds for Promoting Science and Technology from the Ministry of Education, Culture, Sports, Science and Technology (MEXT), and the Core Research Program for Evolutional Science and Technology (CREST) from the Japan Science and Technology Corporation (JST). We are especially grateful to Drs Yuichi Yamasaki, Keiji Itaka, Kensuke Osada, Kanjiro Miyata, Mr Satoru Matsumoto and Mr Shunsaku Asano (The University of Tokyo) for their special technical advice. We thank Dr Makoto Kaneko and Professor Yutaka Yatomi (The University of Tokyo) for supporting us at assessing platelet aggregation. And we also thank Mr Noboru Sunaga Ms Junko Kawakita for their assistance.

References

1 Taniyama Y, Tachibana K, Hiraoka K, Namba T, Yamasaki K, Hashiya N *et al*. Local delivery of plasmid DNA into rat carotid artery using ultrasound. *Circulation* 2002; **105**: 1233–1239.
2 Nishikage S, Koyama H, Miyata T, Ishii S, Hamada H, Shigematsu H. *In vivo* electroporation enhances plasmid-based gene transfer of basic fibroblast growth factor for the treatment of ischemic limb. *J Surg Res* 2004; **120**: 37–46.
3 Edelstein ML, Abedi MR, Wixon J, Edelstein RM. Gene therapy clinical trials worldwide 1989–2004 – an overview. *J Gene Med* 2004; **6**: 597–602.
4 Tomanin R, Scarpa M. Why do we need new gene therapy viral vectors? Characteristics, limitations and future perspectives of viral vector transduction. *Curr Gene Ther* 2004; **4**: 357–372.
5 Wagner E, Ogris M, Zauner W. Polylysine-based transfection systems utilizing receptor-mediated delivery. *Adv Drug Deliv Rev* 1998; **30**: 97–113.
6 Oupicky D, Konak C, Ulbrich K, Wolfert MA, Seymour LW. DNA delivery systems based on complexes of DNA with synthetic polycations and their copolymers. *J Control Release* 2000; **65**: 149–171.
7 Ogris M, Brunner S, Schuller S, Kircheis R, Wagner E. PEGylated DNA/transferrin-PEI complexes: reduced interaction with blood components, extended circulation in blood and potential for systemic gene delivery. *Gene Ther* 1999; **6**: 595–605.
8 Oupicky D, Konak C, Dash PR, Seymour LW, Ulbrich K. Effect of albumin and polyanion on the structure of DNA complexes with polycation containing hydrophilic nonionic block. *Bioconjug Chem* 1999; **10**: 764–772.
9 Katayose S, Kataoka K. Water-soluble polyion complex associates of DNA and poly(ethylene glycol)-poly(L-lysine) block copolymer. *Bioconjug Chem* 1997; **8**: 702–707.
10 Kanayama N, Fukushima S, Nishiyama N, Itaka K, Jang W-D, Miyata K *et al*. A PEG-based biocompatible block catiomer with high buffering capacity for the construction of polyplex micelles showing efficient gene transfer toward primary cells. *ChemMedChem* 2006; **1**: 439–444.
11 Harada-Shiba M, Yamauchi K, Harada A, Takamisawa I, Shimokado K, Kataoka K. Polyion complex micelles as vectors in gene therapy – pharmacokinetics and *in vivo* gene transfer. *Gene Therapy* 2002; **9**: 407–414.
12 Behr JP. The proton sponge. A trick to enter cells the viruses did not exploit. *Chimia* 1999; **51**: 34–36.
13 Kircheis R, Wightman L, Schreiber A, Robitza B, Rossler V, Kursa M *et al*. Polyethyleneimine/DNA complexes shielded by transferrin target gene expression to tumors after systemic application. *Gene Therapy* 2001; **8**: 28–40.

14 Chonn A, Semple S, Cullis P. Association of blood proteins with large unilamellar liposomes *in vivo*. Relation to circulation lifetimes. *J Biol Chem* 1992; **1111**: 239–246.
15 Dash PR, Read ML, Barrett LB, Wolfert MA, Seymour LW. Factors affecting blood clearance and *in vivo* distribution of polyelectrolyte complexes for gene delivery. *Gene Therapy* 1999; **6**: 643–650.
16 Kircheis R, Wagner E. Polycation/DNA complexes for *in vivo* gene delivery. *Gene Therapy Regul* 2000; 1: 95–114.
17 Koyama H, Olson NE, Dastvan FF, Reidy MA. Cell replication in the arterial wall: activation of signaling pathway following *in vivo* injury. *Circ Res* 1998; **82**: 713–721.
18 Koyama H, Olson NE, Reidy MA. Cell signaling in injured rat arteries. *Thromb Haemost* 1999; **82**: 806–809.
19 Clinton SK, Libby P. Cytokines and growth factors in atherogenesis. *Arch Pathol Lab Med* 1992; **116**: 1292–1300.
20 Srinivasan S, Sawyer PN. Role of surface charge of the blood vessel wall, blood cells, and prosthetic materials in intravascular thrombosis. *J Colloid Interface Sci* 1970; **32**: 456–463.
21 Kataoka K, Akaike T, Sakurai Y, Tsuruta T. Effect of charge and molecular structure of polyion complexes on the morphology of adherent blood platelets. *Makromol Chem* 1978; **179**: 1121–1124.
22 Kataoka K, Tsuruta T, Akaike T, Sakurai Y. Biomedical behavior of synthetic polyion complexes toward blood platelets. *Makromol Chem* 1980; **181**: 1363–1373.
23 Seaman GV. Plasma protein interactions at biological interfaces. *Thromb Res* 1983; **(Suppl 5)**: 83–91.
24 Ogris M, Steinlein P, Kursa M, Mechtler K, Kircheis R, Wagner E. The size of DNA/transferrin-PEI complexes is an important factor for gene expression in cultured cells. *Gene Therapy* 1998; **5**: 1425–1433.
25 Mori Y, Nagaoka S, Takiuchi H, Kikuchi T, Noguchi N, Tanzawa H *et al*. A new antithrombogenic material with long polyethylene oxide chains. *Trans Am Soc Artif Intern Organs* 1982; **28**: 459–463.
26 Merrill EW, Salzman EW. Polyethylene oxide as a biomaterial. *ASAIO J* 1983; **6**: 60–64.
27 Llanos GR, Sefton MV. Does polyethylene oxide possess a low thrombogenicity? *J Biomater Sci Polym Ed* 1993; **4**: 381–400.
28 Amiji M, Park K. Prevention of protein adsorption and platelet adhesion on surfaces by PEO/PPO/PEO triblock copolymers. *Biomaterials* 1992; **13**: 682–692.
29 Llanos GR, Sefton MV. Immobilization of poly(ethylene glycol) onto a poly(vinyl alcohol) hydrogel: 2. Evaluation of thrombogenicity. *J Biomed Mater Res* 1993; **27**: 1383–1391.
30 Espadas-Torre C, Meyerhoff ME. Thrombogenic properties of untreated and poly(ethylene oxide)-modified polymeric matrices useful for preparing intraarterial ion-selective electrodes. *Anal Chem* 1995; **67**: 3108–3114.
31 Du H, Chandaroy P, Hui SW. Grafted poly(ethylene glycol) on lipid surfaces inhibits protein adsorption and cell adhesion. *Biochim Biophys Acta* 1997; **1326**: 236–248.
32 Pasche S, Voros J, Griesser HJ, Spencer ND, Textor M. Effects of ionic strength and surface charge on protein adsorption at PEGylated surfaces. *J Phys Chem B* 2005; **109**: 17545–17552.
33 Stary HC, Blankenhorn DH, Chandler AB, Glagov S, Insull Jr W, Richardson M *et al*. A definition of the intima of human arteries and of its atherosclerosis-prone regions. A report from the Committee on Vascular Lesions of the Council on Arteriosclerosis, American Heart Association. *Circulation* 1992; **85**: 391–405.
34 Guzman RJ, Lemarchand P, Crystal RG, Epstein SE, Finkel T. Efficient and selective adenovirus-mediated gene transfer into vascular neointima. *Circulation* 1993; **88**: 2838–2848.
35 Itaka K, Yamauchi K, Harada A, Nakamura K, Kawaguchi H, Kataoka K. Polyion complex micelles from plasmid DNA and poly(ethylene glycol)-poly(L-lysine) block copolymer as serum-tolerable polyplex system: physicochemical properties of micelles relevant to gene transfection efficiency. *Biomaterials* 2003; **24**: 4495–4506.
36 Ozaki Y, Satoh K, Yatomi Y, Yamamoto T, Shirasawa Y, Kume S. Detection of platelet aggregates with a particle counting method using light scattering. *Anal Biochem* 1994; **218**: 284–294.
37 Yamamoto T, Egawa Y, Shirasawa Y, Ozaki Y, Sato K, Yatomi Y *et al*. A laser light scattering *in situ* system for counting aggregates in blood platelet aggregation. *Meas Sci Technol* 1995; **6**: 174–180.
38 Tomida Y, Iino S, Nishikawa M, Hidaka H. A new system to detect native microaggregates of platelets *in vivo*, with a novel platelet aggregometer employing laser light scattering. *Thromb Res* 1998; **92**: 221–228.
39 Misawa Y, Konishi H, Fuse K. Platelet aggregates and cardiopulmonary bypass. *Ann Thorac Surg* 2001; **72**: 981–982.

厚生労働科学研究費補助金

免疫アレルギー疾患予防・治療研究事業

変形性関節症の治療・予防の標的分子の同定とその臨床応用

平成19年度総括研究報告書

第2分冊（2/2）

主任研究者　中村　耕三

平成20年3月

Ⅳ. 研究成果の刊行物・別刷②

Colloid Polym Sci (2007) 285:1055–1060
DOI 10.1007/s00396-007-1660-6

SHORT COMMUNICATION

pH-Responsive PEGylated nanogels as targetable and low invasive endosomolytic agents to induce the enhanced transfection efficiency of nonviral gene vectors

Motoi Oishi · Hisato Hayashi · Keiji Itaka · Kazunori Kataoka · Yukio Nagasaki

Received: 18 December 2006 / Accepted: 3 February 2007 / Published online: 28 February 2007

Abstract A pH-responsive PEGylated nanogel was successfully prepared by means of emulsion copolymerization of 2-(*N*,*N*-diethylamino)ethyl methacrylate (AMA) with heterobifunctional poly(ethylene glycol) (PEG) bearing a 4-vinylbenzyl group at the α-end and a lactose moiety at the ω-end in the presence of potassium persulfate and ethyleneglycol dimethacrylate as a cross-linker. Polyplex micelle composed of PEG-*block*-poly(L-lysine) copolymer and plasmid DNA (PEG-*b*-PLL/pDNA) exhibited a far more efficient transfection ability in the presence of lac-nanogel-8k-1.0% (PEG, M_n=8000; cross-linking density, 1.0%) than the PEG-*b*-PLL/pDNA polyplex micelle alone (in the absence of lac-nanogel-8k-1.0%), suggesting that an appreciable fraction of lac-nanogel-8k-1.0% along with the PEG-*b*-PLL/pDNA polyplex micelle is taken up into the HuH-7 cells through the asialoglycoprotein receptor-mediated endocytosis process mediated by the cluster of a large number of lactose moieties on the surface of lac-nanogel-8k-1.0%, followed by the effective disruption of the endosome by the buffer effect of the unprotonated PAMA core in lac-nanogel-8k-1.0%.

Keywords Core-shell type nanogel · pH-sensitive volume phase transition · Endosomolytic agent · Gene vector · PEG-tethering surface

Electronic supplementary material The online version of this article (doi:10.1007/s00396-007-1660-6) contains supplementary material, which is available to authorized users.

M. Oishi · Y. Nagasaki
Tsukuba Research Center for Interdisciplinary Materials Science (TIMS), University of Tsukuba,
1-1-1 Ten-noudai,
Tsukuba, Ibaraki 305-8573, Japan

M. Oishi · H. Hayashi · Y. Nagasaki (✉)
Graduate School of Pure and Applied Sciences,
University of Tsukuba,
1-1-1 Ten-noudai,
Tsukuba, Ibaraki 305-8573, Japan
e-mail: nagasaki@nagalabo.jp

K. Itaka · K. Kataoka
Division of Clinical Biotechnology,
Center for Disease Biology and Integrative Medicine,
Graduate School of Medicine,
The University of Tokyo,
7-3-1 Hongo, Bunkyo-ku,
Tokyo 113-0033, Japan

K. Kataoka
Department of Materials Engineering,
Graduate School of Engineering, The University of Tokyo,
7-3-1 Hongo, Bunkyo-ku,
Tokyo 113-8656, Japan

Introduction

Nonviral gene delivery systems have recently received increased attention in the field of gene therapy in vivo and ex vivo because of concerns over safety issues related to viral vectors, including immunogenicity, oncogenicity, and potential virus recombination [1–3]. Most of the nonviral vectors developed so far, however, have shown a low transfection efficiency compared to viral vectors because the latter have evolved a multifunctionality, which overcomes one of the critical barrier to efficient gene delivery by enhancing transport to the cytoplasm from the endosomal compartment. Recently, a new class of nonviral gene vectors has been developed based on the supramolecular assembly between plasmid DNA (pDNA) and poly(ethylene glycol) (PEG)-*block*-polyamine copolymers (polyplex micelles) [4–10]. Due to the highly dense PEG shell surrounding the polyion complex (PIC) core, the polyplex

micelles with a size of less than 100 nm exhibited excellent solubility in aqueous media, low cytotoxicity, high tolerability toward nuclease degradation, and minimal interaction with biological components, including proteins and cells, compared to conventional polyplex and lipoplex systems.

Nevertheless, the presence of 100 μM hydroxychloroquine (HCQ) as an endosomolytic agent has so far been required to achieve a high transfection efficiency [2, 11], indicating that endosomal escape should be the most critical barrier to intracellular gene delivery by polyplex micelles [12, 13]. To devise polyplex micelles with a function to escape from the endosome where the pH is 1.4~2.4 units lower than the physiological pH of 7.4 [14–17], poly (ethylenimine) (PEI) derivatives are of interest as an alternative way to accomplish endosomal escape by taking advantage of their substantially lowered value of apparent pK_a (~5.5; "buffer or proton-sponge effect") [18]. However, the buffer effect of the PEI segment occurs only when an excess of amino groups with respect to DNA phosphate groups (high N/P ratio) is present in the system, where a considerable amount of the amino groups in PEI is in free-base form. This fact strongly suggests that free PEI, which is not complexed with pDNA, is likely to play a crucial role in the buffer effect [19, 20]. In addition, both HCQ and free PEI tend to show high toxicity and nonspecific disposition in the body after intravenous injection, viz., the use of HCQ and PEI for the gene therapy under in vitro and ex vivo conditions is still controversial. A major key to the success of nonviral gene delivery system is believed to be the development of targetable and low invasive endosomolytic agents, which can achieve the low cytotoxicity and modulated disposition in the body as well as the smooth accumulation into the target cell.

Worth noting in this regard is a new class of pH-responsive PEGylated nanogels constructed from a cross-linked pH-sensitive polyamine core and tethered PEG chains bearing a carboxylic acid group as a platform moiety to install ligand molecules [21]. The pH-responsive nanogels showed excellent stability under physiological conditions and significant volume phase transition (swelling) in response to endosomal pH (pH>7.5, diameter ca. 80 nm; pH<6.5, diameter ca. 150 nm; see Fig. S1) due to the protonation of the cross-linked polyamine core surrounded by the tethered PEG chains, indicating that the cross-linked polyamine core of the nanogels acts as a buffering moiety for facilitated endosomal escape. A unique finding, which we would like to communicate in this paper, is the remarkably enhanced transfection efficiency without cytotoxicity in cultured hepatoma cells through the PEGylated polyplex micelle composed of PEG-*block*-poly (L-lysine) copolymer (PEG-*b*-PLL: $M_{n\ PEG}$=12,000, $M_{n\ PLL}$=11,600) and pDNA along with pH-responsive lactosylated nanogel (Fig. 1); thus, the pH-responsive lactosylated nanogel is promising as a targetable and

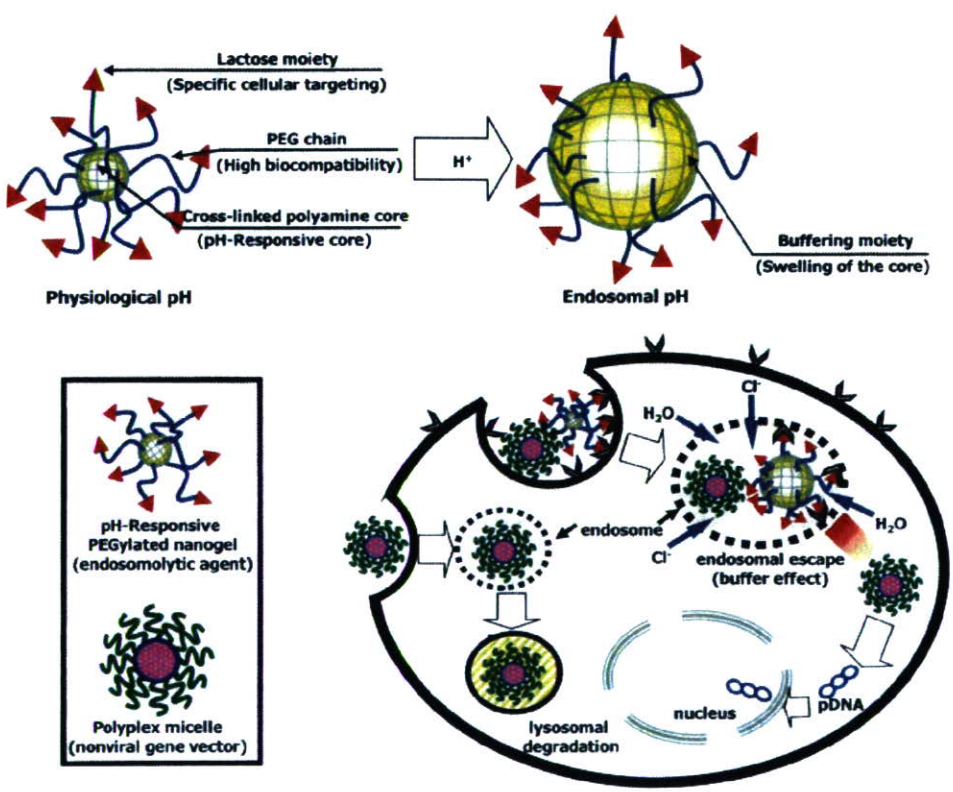

Fig. 1 Schematic illustration of the pH-responsive PEGylated nanogel and endosomal escape mechanism

biocompatible endosomolytic agent for nonviral gene delivery systems.

Experimental

General Ethylene glycol dimethacrylate (EGDMA; Wako) and 2-(*N*,*N*-diethylamino)ethyl methacrylate (AMA, Wako) were distilled over CaH_2 under reduced pressure. Potassium persulfate (KPS; Wako) was purified by recrystallization from water and then dried in vacuo. Asialofetuine (ASF) and HCQ were purchased from Sigma and Acros Organics, respectively. Water was purified using the Milli-Q system (Millipore). Plasmid DNA (pDNA) encoding firefly luciferase (pGL3-Luc, Promega; 5,256 bpa) was amplified using EndoFree™ Plasmid Maxi or Mega Kits (Qiagen). The DNA concentration was determined by reading the absorbance at 260 nm. Dynamic light scattering (DLS) measurements were carried out using a light-scattering spectrometer (DLS-7000, Otsuka Electronics. Japan) equipped with a vertically polarized incident beam at 488 nm supplied by an argon ion laser at scattering angles of 90°. Lasser–Doppler electrophoresis measurements of the PEGylated nanogels were carried out in 10 mM $NaCl_{aq}$ (ELS-600, Photal, Otsuka Electronics).

Synthesis of CH_2=CH–Ph–PEG–lactose and preparation of nanogels Heterobifunctional α-vinylbenzyl-ω-carboxyl-poly(ethylene glycol) [CH_2=CH–Ph–PEG–COOH; molecular weights (MW): 2k and 8k] macromonomers were synthesized in accordance with our previous report [21]. To a solution of potassium 4-vinylbenzyl alcoholate (0.5 mmol) in tetrahydrofolate (THF; 20 ml), 22.7 mmol (1.1 ml) of ethylene oxide were added under an argon atmosphere. After the reaction mixture was stirred at room temperature for 2 days, 2.5 mmol (3.4 ml, 0.725 mol/l in THF solution) of succinic anhydride was added to introduce a carboxylate group at the ω-end. After the purification of CH_2=CH–Ph–PEG–COOH, lactose was installed at the carboxylic acid group of CH_2=CH–Ph–PEG–COOH through an activated ester method, viz., 8.0 mg of CH_2=CH–Ph–PEG–COOH (MW: 8k, 10 μmol) were reacted with 22 mg of *p*-aminophenyl-β-D-lactopyranoside (50 μmol) in the presence of 250 μmol of *N*-hydroxysuccinimide (NHS) and 1.25 mmol of 1-ethyl-3-(3-dimethylaminopropyl)carbodiimide, hydrochloride (EDC; NHS/EDC ratio of 1:5) in 25 mM 2-morpholinoethanesulfonic acid (MES) buffer (10 ml), pH 6.5. The reaction mixture was stirred at room temperature for 24 h. The CH_2=CH–Ph–PEG–lactose was precipitated in cooled 2-propanol (twice) and dialyzed (MWCO: 3,500) against distilled water for 2 days. The CH_2=CH–Ph–PEG–lactose was finally freeze-dried from water to quantitatively obtain the white powder. We used a typical procedure for the preparation of the pH-responsive nanogels possessing a lactose moiety at the PEG chains, as follows: after 65 mg (8.1 μmol) of the obtained CH_2=CH–Ph–PEG–lactose (8k) were loaded into the reactor, the vacuum and argon purging cycles were repeated three times, followed by the successive addition of deionized/distilled water (1.5 ml), 130 μg of 2-(*N*,*N*-diethylamino) ethyl methacrylate (AMA, 141 μl, 700 μmol) and 1.5 μl of ethyleneglycol dimethacrylate (EGDMA, 7.1 μmol). Emulsion copolymerization was initiated with the addition of 1 ml of aqueous KPS (7.2 mM). The mixture was allowed to react at room temperature for 24 h with stirring. The nanogel was purified by dialysis against distilled water for 2 days.

Cytotoxicity assay Human hepatocarcinoma cells (HuH-7) were seeded onto 96-well plates at a seeding density of 8×10^3 cells/well. The cells were maintained in Dulbecco's modified Eagle's medium (DMEM) supplemented with 10% fetal bovine serum (FBS) and 1.0% penicillin–streptomycin for 24 h at 37 °C in a humidified atmosphere under 5% CO_2. Then, the culture medium was replaced by 90 μl of fresh medium containing serum and antibiotic, followed by the addition of 10 μl of the nanogels at various concentrations. After 24 h, 100 μl of 3-(4,5-dimethylthiazol-2-yl)-2,5-diphenyl tetrazolium bromide (MTT assay, cell counting kit; Dojindo) stock solution in culture medium were added to each well. After an additional 4 h of incubation, the viability of the cells in each well was measured following the protocol provided by the manufacturer. The results are expressed as means±SEM, $n=8$.

Transfection study To a pDNA (pGL3-Luc, Promega; 5,256 bps) solution in 10 mM Tris–HCl buffer (pH 7.4), PEG-*block*-poly(L-lysine) (PEG-*b*-PLL: $M_{n\ PEG}=12{,}000$, $M_{n\ PLL}=11{,}600$), the block copolymer solution in the same buffer, was added at the charge ratio of lysine units vs nucleotide equals 2 (N/P=2) to prepare the polyplex micelle. The HuH-7 cells were seeded in 24-well culture plates at a seeding density of 2.5×10^4 cells/well. After a 24-h incubation in a medium containing 10% FBS, the cells were rinsed, and then 250 μl of the culture medium containing 100 μg/ml of lac-nanogel-8k along with the PEG-*b*-PLL/pDNA polyplex micelle solution (25 μl/well; pDNA concentration, 30 μg/ml) were added to each well. After 24 h, the medium was removed and then replaced with the culture medium. The luciferase gene expression was measured after a further 24 h of culturing. For the competitive inhibition assay of lac-nanogel-8k to the asialoglycoprotein (ASGP) receptor on the HuH-7 cells, a medium containing 1.5 mg/ml of ASF was added to the culture system 30 min before the transfection study. The cells were lysed, and the luciferase activity of the lysate